Nanoscale Advances

ROYAL SOCIETY OF CHEMISTRY

REVIEW

View Article Online
View Journal | View Issue

Cite this: *Nanoscale Adv.*, 2026, **8**, 1791

Role of sodium borohydride as a co-catalyst for nanoparticle-induced degradation of toxic dyes in aquatic systems

Priyadarshni Nathawat,[a] Mamta Sahu[b] and Mainak Ganguly *[b]

The remarkable catalytic and sensing capabilities of metal nanoparticles and nanoclusters have garnered much interest. They are perfect for environmental applications because of their high surface-to-volume ratio and adjustable surface chemistry. Pollution, especially from organic pollutants like synthetic colours, causes major ecological and health risks in addition to other environmental problems. The most common catalyst among the different transition metals is silver in the form of nanoparticles and nanoclusters, with sodium borohydride ($NaBH_4$) serving as a co-catalyst. The catalytic behaviour of nanoparticles and nanoclusters in the presence of $NaBH_4$ is highlighted in this research. This review paper illustrated the function of $NaBH_4$ in dye degradation, covering the removal mechanism, reaction ordering, reaction kinetics and influence of co-catalysts under different physicochemical conditions. These review articles will hopefully be an asset for new researchers working in the field of sustainable water management and nanocatalysts with a clarified idea of reductive photocatalysts with sodium borohydride. In order to facilitate quick electron transfer to dye molecules and accelerate their degradation, sodium borohydride acts as an electron donor and experiences surface oxidation on metal catalysts.

Received 28th January 2026
Accepted 8th February 2026

DOI: 10.1039/d6na00073h

rsc.li/nanoscale-advances

1. Motivation

Due to its strong reducing capacity and quick electron-donating characteristics, sodium borohydride ($NaBH_4$) has been widely used in dye degradation investigations. It is very successful at reducing a variety of organic dye compounds. Several experimental studies have shown how effective it is at changing and decolorising resistant dyes, either on its own or in conjunction with catalytic systems. The use of $NaBH_4$ in dye degradation processes has been documented in a large number of research articles, but there aren't many specialised review papers that methodically gather, analyse, and critically assess its mechanistic role, efficiency, limitations, and comparative performance in such systems. In contrast, a lot of research has been done on the breakdown of dyes using hydrogen peroxide

[a]*Department of Biosciences, Manipal University Jaipur, Dehmi Kalan, Jaipur 303007, India*

[b]*Solar Energy Conversion and Nanomaterials Laboratory, Department of Chemistry, Manipal University Jaipur, Dehmi Kalan, Jaipur 303007, India. E-mail: mainak.ganguly@jaipur.manipal.edu*

Priyadarshni Nathawat

Priyadarshni Nathawat received her BSc and MSc degrees from International College of Girls (ICG), IIS (Deemed to be) University (Jaipur, India). She is currently pursuing her PhD degree under the supervision of Dr Mainak Ganguly in the Department of Biology at Manipal University, Jaipur (India). Her areas of research are environmental nanotechnology, waste recycling, phytochemistry and spectroscopy.

Mamta Sahu

Mamta Sahu received her BSc degree from S. S. Jain Subodh Girls P. G. College (Jaipur, India) and MSc from R. K. Vigyan Mahavidyalaya (Jaipur, India). She is currently pursuing her PhD degree under the supervision of Dr Mainak Ganguly in the Department of Chemistry at Manipal University, Jaipur (India). Her areas of research are environmental nanoscience and spectroscopy.

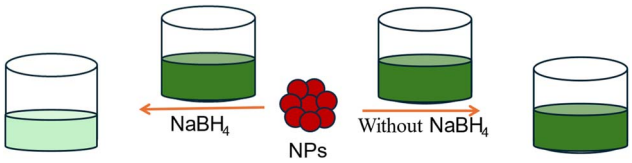

Scheme 1 Degradation of dye with and without sodium borohydride.

(H_2O_2), a common oxidising agent.[1] Because of its use in advanced oxidation processes (AOPs), a number of thorough reviews and research publications describing reaction pathways, catalyst systems, operational parameters, and environmental consequences have been published. A substantial knowledge gap in $NaBH_4$-based reduction techniques for dye degradation is shown by this imbalance in the literature. The current review (Scheme 1) is therefore highly focussed on closing this gap by methodically emphasising the significance of $NaBH_4$ as a powerful reducing agent, critically examining its function, mechanisms, benefits, and difficulties in dye degradation, and situating it within the larger framework of environmental remediation and wastewater treatment technologies.

2. Introduction

An important natural resource for both life and the development of technology is water. However, because numerous enterprises release wastewater for a variety of purposes worldwide, growing industrialisation has greatly increased aquatic pollution, as mentioned in Table 1.[2–4] Significant sources of pollution include the electrochemical industries, which include the production of batteries, electroplating, and chlor-alkali. Toxic metals such as lead, cadmium, mercury, chromium, and cyanides are released into water bodies by these processes, frequently in excess of permissible levels. Metal pollution in aquatic systems is also exacerbated by corrosion brought on by carbonates and chlorides in water, which is an electrochemical process in and of itself.[4–8] Significant global water and soil pollution has resulted from the fast rise in industrial effluent discharge, mostly as a result of the presence of persistent organic pollutants, including dyes, pesticides, and phenolic compounds. Even at low quantities, synthetic dyes, especially those emitted by the paper, pharmaceutical, food processing, textile, and cosmetic sectors, pose serious dangers to human health and the environment. Ten percent or more of these dyes are left untreated during industrial processing, which has detrimental effects on the environment. Their persistence in aquatic systems disrupts aquatic photosynthesis and puts aquatic animals at risk by changing the colour of the water, decreasing light penetration, decreasing the amount of dissolved oxygen available, and increasing biological oxygen demand (Table 1). Because of their mutagenic and carcinogenic qualities, azo dyes are especially concerning among them. This highlights the urgent need for sophisticated treatment methods and strict control to lessen their negative effects.[9–20]

The expanding potential of nanomaterials in water treatment, particularly for poorer nations where affordability is essential, such as India and other developing countries, holds promise. Because they use fewer raw materials, use less energy, and are more ecologically friendly, especially when made with green chemistry principles, nanomaterials have benefits over traditional technology. However, due to a lack of quantitative evidence about long-term advantages and worries about the effects of nanoparticles on the environment and human health, their broad adoption is still up for debate. Notwithstanding these reservations, nanomaterials have the potential to provide effective, reasonably priced, and environmentally friendly water purification solutions through their use as sorbents, catalysts, and nanofiltration membranes.[21]

For the destruction of organic contaminants in water, photocatalysis is a popular and sustainable environmental remediation technique. In this process, light energy is absorbed by a photocatalyst (usually a semiconductor material like TiO_2, ZnO, or g-C_3N_4), which then produces electron–hole pairs when exposed to photons of the right energy.[22] These photogenerated charge carriers go to the surface of the catalyst, where they take part in redox processes and create reactive species that can break down organic pollutants. Co-catalysts are frequently added to the system to improve photocatalytic performance. Co-catalysts facilitate effective charge separation, inhibit electron–hole recombination, and accelerate surface redox processes. They can be chemical agents like $NaBH_4$ and H_2O_2 or metal nanoparticles like Ag, Au, and Fe. Since catalytic activity is maintained by the quick and focused transport of electrons from the photocatalyst to the co-catalyst or directly to adsorbed pollutant molecules, electron transfer is a crucial mechanistic element controlling photocatalytic efficiency. When co-catalysts are added, favourable electron transfer paths are created, which speed up electron shuttling, reduce recombination losses, and eventually result in much higher photocatalytic degradation efficiency.[23]

3. Nanoclusters V/S nanoparticles

This section discusses the difference between nanoparticles (NPs) and metal nanoclusters (NCs). Nanoparticles are unique

Mainak Ganguly

Dr Mainak Ganguly received his PhD from the Indian Institute of Technology, Kharagpur, India, in 2014. He also has 5 years of postdoctoral research experience at Furman University (USA) and McGill University (Canada). He is currently working as an Associate Professor in the Department of Chemistry, Manipal University, Jaipur (India). His research interests include nanoparticles, clusters, biophysical chemistry, environmental remediation, etc. He has published more than 90 papers.

Table 1 Types of pollutants, their sources and effects

Pollutant type	Examples	Sources	Effects
Heavy metals	Lead, cadmium, mercury, chromium	Batteries, tanneries, mining	Bioaccumulation, carcinogenic, organ damage
Organic dyes	Indigo, henna, methylene blue	Textile, paper, cosmetic industries	Toxicity, mutagenicity, reduced light penetration
Plastic pollution	One-time use plastic, microplastic	Fishing net, packing dispatches	Consumption of marine life, bioaccumulation, ecological imbalance, and pollution of soil and water
Biological factors (example: bacteria, algae)	*Salmonella*, *E. coli*, cyanobacteria	Sewage, food, water, and animal waste that are contaminated and eutrophication	Food poisoning, cholera, typhoid, and nausea. Aquatic animal toxicity, liver damage, and skin irritation

due to their larger surface area (1–100 nm). One such property is surface plasmon resonance (SPR), which occurs when light interacts with the electrons on the surface of the nanoparticle. By comparison, metal nanoclusters are much smaller (about 2 nm) and only contain tens to hundreds of atoms. Because of their tiny size, nanoclusters lack the surface area necessary for surface plasmon resonance (SPR) but have properties more like molecules, such as luminescence and catalysis. To put it simply, nanoclusters serve as a conduit between the activities of individual atoms and larger nanoparticles.[24] Nanoparticles (NPs) may endure numerous reaction cycles, are structurally stable, and do not aggregate. They are appropriate for direct use in wastewater treatment facilities because they may be produced in large quantities at a reasonable cost. Additionally, NPs retain their catalytic activity in the presence of high pollutant concentrations, fluctuating pH levels, and extended radiation exposure. They are very versatile since their composition and shape (spheres, rods, and cubes) can be changed to adjust their photocatalytic activity. Because they strike a compromise between durability, cost, and efficiency, NPs are already widely used in the degradation of dyes and pollutants. Nanoclusters (NCs), on the other hand, are extremely small (less than 2 nm), frequently unstable, and oxidation prone. They need protective ligands or support, like polymers or TiO_2 sheets, to stop degrading. Their synthesis necessitates exact control, which is costly and challenging to scale. Additionally, NCs tend to deteriorate or leak in adverse environments, which restricts their long-term applicability. NCs are primarily researched as advanced model catalysts and are more composition-restricted than NPs. Although they provide extremely high catalytic efficiency in well-regulated lab settings, their practical implementation is fraught with difficulties.[25,26]

4. Dye degradation

There are a variety of dyes (Fig. 1), and in chemistry, dyes have a variety of uses. They are used as colourants, reactants, indicators, and catalysts in organic synthesis, catalysis, photocatalysis, and materials science processes. Recent research highlights how they work with nanocatalysts to clarify reaction kinetics and mechanisms, especially in clock reactions and advanced oxidation processes. Many industrial uses, such as textiles, inkjet printing, and analytical chemistry, rely on aromatic and heterocyclic dyes, whereas reactive dyes are prized for their ability to establish covalent bonds with substrates like cellulose and synthetic fibres, allowing for long-lasting colouration. In photochemical and environmental applications, dyes also serve as redox agents and photosensitizers. This is particularly true in wastewater treatment, where learning how dyes degrade due to radicals is essential to creating long-term remediation plans.[27–31] The high specific surface area and plentiful active sites of the catalysts used in dye treatment systems enable effective adsorption of dye molecules and accelerate the rates of dye breakdown. Catalysts also facilitate sophisticated oxidation processes, which allow dyes to be efficiently mineralised into ecologically safe final products. By enhancing the separation and conveyance of photogenerated charge carriers, the addition of co-catalysts, such as metal nanoparticles or appropriate chemical agents, further improves catalytic efficiency. By acting as charge-transfer mediators or electron sinks, these co-catalysts greatly boost the overall reaction rate and degradation efficiency by preventing electron–hole recombination.[32,33]

4.1 Methylene blue

The strong blue colour and redox adaptability of methylene blue (MB) are caused by its planar, cationic aromatic structure, which is a heterocyclic phenothiazine derivative. MB was first created as a textile dye, but it has subsequently been used in biology, medicine, and environmental science. Its reversible redox cycling with leucomethylene blue supports its functions in catalysis, electron transport, and therapy (such as the

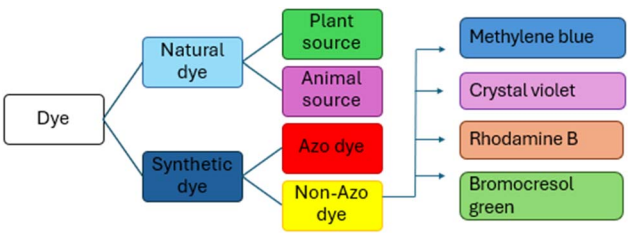

Fig. 1 Using a flowchart, the figure classifies various dyes according to their chemical components and place of origin.

treatment of methemoglobinemia). In studies of adsorption and photocatalytic degradation, the molecule serves as a reference dye, a fluorescent probe in imaging, and a photosensitiser in photodynamic treatment. Clinical applications for MB include antibacterial, antimalarial, diagnostic stain, surgical marker, and new neuroprotective techniques. In terms of the environment, it is frequently used as a model contaminant in studies on water purification; however, discrepancies in published physicochemical data underscore the necessity of standard operating procedures. Although it has a wide range of applications, its toxicity at higher concentrations calls for careful use.[34–37]

4.2 Crystal violet

A cationic triphenylmethane dye ($C_{25}H_{30}N_3Cl$, crystal violet (CV)) is utilised extensively in materials research, biological staining, and microbiological detection because of its excellent visible light absorption, vivid violet colour, and remarkable nonlinear optical characteristics. It can improve the dielectric, piezoelectric, and thermal characteristics of host crystals like ADP and KDP in addition to its initial usage as a textile dye. It also finds utility in optoelectronic and sensing devices. Environmental problems arise from its persistence and resistance to biodegradation, yet its strong affinity for negatively charged surfaces makes it useful in adsorption and environmental investigations. The need for cautious handling and efficient wastewater cleanup techniques is further highlighted by the fact that CV is known to have toxic, genotoxic, and possibly carcinogenic effects. Numerous studies have been conducted on the removal of CV from wastewater utilising inexpensive adsorbents such as carbon nanotubes, grapefruit peels, and industrial wastes. Because of its high optical activity, it is used in nonlinear optics, lasers, and sensor technologies.[38–43]

4.3 Rhodamine B

Rhodamine B (RhB) is a synthetic cationic dye based on xanthene that is widely used in materials science, textiles, food colouring, and biological staining because of its bright pink-red fluorescence, which allows for a wide range of applications in microscopy, spectroscopy, and sensing. Enhancing its functional flexibility are its water solubility and π–π and electrostatic interactions with a variety of substrates. Significantly, RhB is a potential element in smart materials and sensor technologies due to its stimuli-responsive chromic behaviour, which manifests as colour and fluorescence variations under various environmental conditions. Although it is frequently found in textile wastewater, RhB is also known to be a persistent and hazardous contaminant that is resistant to biodegradation and may be carcinogenic and mutagenic. With growing interest in photoelectrocatalysis and nanostructured adsorbents as sustainable remediation techniques, a significant amount of research has been devoted to creating effective removal strategies, such as adsorption and photocatalytic degradation employing nanomaterials, activated carbons, and sophisticated photocatalytic systems.[44–47]

4.4 Bromocresol green

A triphenylmethane dye of great analytical significance, bromocresol green (BCG) is mostly used as a pH indicator and biochemical reagent because of its characteristic colour shift from yellow in acidic (pH < 3.8) to blue–green in alkaline (pH > 5.4) environments. Due to its ionisable molecular structure, which promotes stable compound formation with proteins, BCG has a significant absorbance maximum at 616 nm under alkaline conditions. It also has low solubility in water but increased solubility in alcohols. Its broad use in biochemical tests, such as serum albumin measurement, is supported by this property. Its relevance in analytical chemistry has expanded due to recent studies on its thermodynamic and aggregation behaviours, which have shown that interactions with solvents like alcohols and diols significantly alter its spectrum and binding characteristics.[48–51] Beyond its use in laboratories, BCG has been integrated into intelligent food packaging systems as a pH-sensitive indicator for real-time freshness monitoring, particularly in fish products. Studies on its removal from wastewater through adsorption using agricultural byproducts like rice husks and corn cobs have also highlighted its environmental relevance. Its flexibility in clinical, environmental, and industrial domains is further demonstrated by its ability to form ion–pair complexes with pharmaceutical molecules, which permits its use in spectrophotometric drug testing, namely for quality control of antihypertensives.[52]

5. Sodium borohydride ($NaBH_4$)

Different structures of $NaBH_4$ have been reported in the literature. Under ambient conditions (STP), the cubic R-phase is the most stable phase. The R-phase exists at low temperature, while the γ-phase is only observed at high pressure.[53–60] The stability of $NaBH_4$ is discussed in the paragraph as being crucial for its application in portable hydrogen generators, especially in low-temperature fuel cells for transportation. $NaBH_4$ solutions provide a cleaner substitute for gasoline since they can hydrolyse hydrogen. $NaBH_4$ hydrolysis, however, produces sodium hydroxide (NaOH) during storage, which raises pH and inhibits more hydrolysis. Temperature and pH have the biggest effects on the rate of hydrolysis, which is slower in alkaline environments. For dependable industrial use, additional information on storage parameters particularly temperature and the hydrolysis rate is crucial, even though $NaBH_4$ solutions with water and NaOH are more stable over time. Understanding these characteristics during periods when hydrogen production is not active is the main goal of this work. In the process of creating nanoparticles, $NaBH_4$ fulfils several vital roles.[10–16] It is a powerful reducing agent that, even at room temperature, quickly converts metal salts to their elemental metal form. By causing an abrupt burst of nucleation that aids in the creation of homogeneous nanoparticles, its quick reduction kinetics are also essential for nucleation control. Moreover, particle size regulation is influenced by $NaBH_4$; with higher concentrations, smaller, more monodisperse particles tend to form. In some situations, it also aids in stabilisation since the borate

byproducts produced during the reaction have the ability to adhere to the surface of the nanoparticles and stop them from aggregating. Additionally, $NaBH_4$ demonstrates the capacity to reduce some metal ions more easily than others.[61–63]

The decomposition technique, which frequently makes use of heat, catalysts, or chemical processes, entails disassembling a complex into simpler chemicals or components. In the context of chemical processing or water treatment, this usually entails dissolving contaminants or reactants into forms that are safer or easier to handle.[64,65] Along with a nanocatalyst, H_2O_2 or $NaBH_4$ is often used for dye degradation as a co-catalyst. H_2O_2 and $NaBH_4$ are both unstable under reaction conditions. The decomposition of H_2O_2 is mentioned in eqn (1) and (2).[66]

Decomposition of hydrogen peroxide

$$2H_2O_2 \rightarrow 2H_2O + O_2 \quad (1)$$

Hydrolysis of sodium borohydride

$$NaBH_4 + 2H_2O \rightarrow NaBO_2 + 4H_2\uparrow \quad (2)$$

The mechanistic features of $NaBH_4$ hydrolysis on face-centred cubic cobalt (fcc-Co) surfaces were investigated using density functional theory (DFT) simulations, with a focus on the involvement of surface-adsorbed hydroxyl ($^{\bullet}OH$) radicals. Because of its ideal surface coordination and electronic structure, the Co(III) surface has the best adsorption energetics and the lowest activation barriers for $NaBH_4$ breakdown, according to periodic slab models of low-index cobalt facets. Metal-to-borohydride electron transfer during adsorption on Co(III) significantly weakens B–H bonds, allowing progressive hydride abstraction and hydrogen development. Surface hydroxyl radicals were found to have a significant impact on the reaction energy landscape, while excessive $^{\bullet}OH$ adsorption causes surface crowding and kinetic inhibition, and moderate $^{\bullet}OH$ coverage stabilises transition states through hydrogen bonding and electrostatic interactions, thereby lowering activation barriers. In line with a surface-assisted, stepwise reaction route, the hydrolysis progresses through thermodynamically stable intermediates like $NaBH_3OH$ and $NaBH_3O$. Strong hybridisation between Co d-orbitals and borohydride species is revealed by electronic density of states analysis, which facilitates effective electron transport and explains cobalt's high catalytic activity. In general, the work offers an atomic-level understanding of how hydroxyl species and surface structure control hydride activation and reaction kinetics during $NaBH_4$ hydrolysis.[67]

The pH of the solution has a significant impact on the speeds at which this reaction progresses and produces hydrogen gas. Because protonation of the hydride (BH_4^-) promotes quicker bond breakage and hydrogen evolution, the hydrolysis rate is greatly enhanced under very acidic or neutral conditions. The BH_4^- ion, on the other hand, is more stable in alkaline solutions, and hydrolysis proceeds much more slowly because basic media have better borohydride stability and less proton availability. Therefore, alkaline conditions (*e.g.*, pH > 10) extend the half-life of $NaBH_4$ solutions and prevent fast breakdown, making them more appropriate for regulated applications like catalytic processes or hydrogen storage. While lower pH settings accelerate hydrogen evolution and increase the protonation of BH_4^-, raising pH generally increases the reaction activation energy and decreases the rate constant of $NaBH_4$ hydrolysis. Additionally, experimental findings demonstrate that the self-hydrolysis of $NaBH_4$ causes the pH of the solution to rise as the hydrolysis proceeds, ultimately generating a borate buffer around pH ~9.4–9.5, which subsequently slows down additional hydrolysis and hydrogen generation. Hydrolysis kinetics in acidic environments may be described as pseudo-first-order concerning $NaBH_4$, and the rate constants are often greater than in alkaline systems.[68,69]

5.1 Applications of $NaBH_4$

5.1.1 Organic chemistry and the pharmaceutical industry. In organic chemistry, $NaBH_4$ is a widely used and versatile reducing agent that selectively reduces carbonyl functional groups. It most frequently converts aldehydes and ketones into their corresponding primary and secondary alcohols under mild conditions through hydride ion attack on the electrophilic carbonyl carbon followed by protonation. This transformation is fundamentally important in chemical synthesis because it provides an effective, controllable, and highly selective route for producing a wide range of alcohols. As a result, it is widely used in both laboratory and industrial processes, including the synthesis of pharmaceuticals, fine chemicals, and functional materials.[70,71]

5.1.2 Industrial applications. Sulphur dioxide (SO_2) is converted to sodium dithionite ($Na_2S_2O_4$) in the pulp and paper industry using sodium borohydride ($NaBH_4$) as a reducing agent. Due to its ability to selectively remove chromophoric groups in lignin without causing significant breakdown of cellulose fibres, sodium dithionite is a commonly used bleaching chemical for wood pulp. The mechanical strength of the paper is maintained while pulp brightness and quality are improved. As a result, the use of sodium borohydride in the *in situ* manufacturing of sodium dithionite is of significant industrial significance, supporting effective, superior, and ecologically sustainable paper manufacturing processes.[72]

5.1.3 Environmental and energy applications. The strong reducing capabilities of $NaBH_4$, which allow the transformation and detoxification of a wide spectrum of hazardous contaminants, have garnered significant interest in wastewater treatment. Toxic organic molecules, dyes, and certain heavy metal ions may all be successfully reduced by it, which lessens their ecological impact and environmental persistence. Additionally, by inactivating dangerous bacteria and enhancing overall effluent quality, $NaBH_4$-assisted reduction operations can aid in wastewater disinfection, contributing to pollution control and environmental protection.[73]

5.1.4 Hydrogen storage. Sodium borohydride has a large gravimetric hydrogen content, and has also been thoroughly studied as a potential hydrogen storage material. In the presence of appropriate catalysts, $NaBH_4$ hydrolyses to produce sodium metaborate as a byproduct while releasing hydrogen

Table 2 Comparison between reagents $NaBH_4$, $K_2S_2O_8$ and H_2O_2

Properties	Sodium borohydride	Potassium persulfate	Hydrogen peroxide
Nature of chemical	Reducing	Strongly oxidizing	Oxidizing
Decomposition	$NaBO_2 + H_2$	SO_4^{2-} + free radicals	$H_2O + O_2$
Toxicity	Releases flammable gas, corrosive	Oxidizer: causes irritation in eyes and on skin	Explosive at high concentration

gas in a regulated way. Because of its capacity to produce hydrogen on demand, sodium borohydride is a promising option for hydrogen supply in fuel cell technologies and portable energy systems, underscoring its potential contribution to clean and sustainable energy applications.[74]

6. Co-catalysts

A chemical species known as a co-catalyst works in tandem with a primary catalyst to enhance a catalytic system's overall performance. It performs an auxiliary function by renewing the active catalytic sites, altering the reaction environment, or enabling other mechanistic paths, in contrast to the primary catalyst, which starts the process directly. By speeding up the overall reaction rate, improving selectivity by guiding the catalyst towards particular reaction pathways, stabilising the catalyst by preventing deactivation, and supplying necessary intermediates like electrons, protons, or other reactive species needed to maintain the catalytic cycle, the addition of a co-catalyst can greatly increase catalytic efficiency.[75,76]

6.1 Comparison of co-catalysts

As a well-known strong reducing agent, sodium borohydride ($NaBH_4$) is helpful in a variety of chemical processes since it easily transfers electrons to other molecules. It is fairly robust in its solid (dry) state and is resistant to degradation at temperatures as high as 400 °C. It is only stable in alkaline (basic) solutions when dissolved in water, though, and breaks down gradually under these conditions. Sodium metaborate ($NaBO_2$) and hydrogen gas (H_2) are the primary byproducts of this breakdown. Because it is corrosive and generates hydrogen gas, which is extremely combustible and dangerous for explosions, $NaBH_4$ must be handled cautiously even if it is quite successful in chemical reductions. A potent oxidising agent, potassium persulfate ($K_2S_2O_8$) readily takes electrons from other materials and initiates potent chemical reactions. At temperatures exceeding 100 °C, it remains stable, but at around 120 °C, it begins to degrade. Sulphate ions (SO_4^{2-}) and very reactive free radicals are produced during this breakdown. In advanced oxidation processes (AOPs), which are techniques used to break down or eliminate contaminants from water and the environment, these radicals are very helpful. $K_2S_2O_8$ must be treated carefully, nevertheless, because of its potent oxidising ability, which can be hazardous to people and cause skin and eye irritation. At about 150 °C, hydrogen peroxide (H_2O_2), a frequently used oxidising agent, thermally breaks down to produce oxygen (O_2) and water (H_2O). Under normal conditions, it decomposes somewhat slowly in aquatic settings, but the presence of transition metal catalysts (such as Fe^{2+} and Cu^{2+}) can significantly speed up this process. Its use in Fenton and photo-Fenton procedures, which produce very reactive hydroxyl radicals ($^{\bullet}OH$) for the effective destruction of organic contaminants, is supported by this catalytic activation. Although hydrogen peroxide is less intrinsically stable than persulfates, its reactivity and capacity to produce radicals make it a flexible oxidant in a variety of industrial and environmental settings. It is typically safe to handle at low concentrations, but at high concentrations, its tremendous oxidising power and dramatic decomposition potential, which if not well controlled, might lead to explosive events, posing serious risks. A comparative study is mentioned in Table 2.[75–84]

6.2 Advantages and disadvantages of $NaBH_4$ as a co-catalyst

Sodium borohydride ($NaBH_4$) is a very efficient reducing agent that is widely employed in catalytic reduction and chemical synthesis. In its dry state, it has selective reducing activity towards aldehydes, ketones, and certain metal ions and is thermally stable up to about 400 °C. It can also break down to produce hydrogen gas, which could have uses in energy systems. Unfortunately, $NaBH_4$ decomposes quickly outside of alkaline conditions and is only stable in aqueous solutions. Strict handling precautions are necessary due to the corrosive nature of the breakdown, which generates flammable hydrogen gas that poses a risk of explosion. Its extensive use is further restricted by its comparatively high cost in comparison to other reducing agents.[85–91] Although sodium borohydride ($NaBH_4$) has been thoroughly studied as a material for storing hydrogen, a number of restrictions prevent its widespread use. Its commercial viability is diminished by the high energy and expense of $NaBH_4$ production and regeneration, as well as the lack of effective recycling techniques. While solid $NaBH_4$ is rather stable, its hydrolysis requires catalysts and controlled conditions, as it is extremely reactive with water, making safe storage and handling problematic, particularly under humid conditions. Transition metal catalysts like cobalt, nickel, or platinum are often required for efficient hydrogen generation; however, their long-term performance is limited by their high cost and susceptibility to deactivation by sintering or poisoning. Moreover, sodium metaborate ($NaBO_2$) is a byproduct of hydrolysis that adds obstacles to sustainable use and complicates regeneration cycles. In comparison to other hydrogen carriers like ammonia borane and liquid organic hydrogen carriers, $NaBH_4$ exhibits inferior energy efficiency when assessed over its whole life cycle, which includes manufacturing, storage, and regeneration. Its practical implementation is further hampered by the need to transport both

Table 3 Synthesis of nanoparticles for dye degradation with $NaBH_4$ as a co-catalyst

Nanoparticles	Precursor	Condition	Size and shape	Application	References
FeNPs	($FeCl_3 \cdot 6H_2O$), *Vernonia amygdalina* leaf extract, ethanol	Room temperature	(1–4 μm) average particle size 2.31 μm	Catalytic degradation of methylene blue and crystal violet dye	69
AuNPs	$AuCl_3 \cdot HCl \cdot 4H_2O$, polyvinyl alcohol, polydopamine, sodium alginate, $CaCl_2$-saturated boric acid, HCl, $CaCO_3$, dopamine	Room temperature	Spherical in shape and diameter ranging from 5 to 60 nm	Degradation of rhodamine B	102
AgNPs	*Imperata cylindrica*, $AgNO_3$	Heat (water bath) at 60 °C for 10 min	Average particle size was 31 nm	Degradation of methylene blue dye	103
Ag NPs, Ni NPs, Cu NPs	($CuCl_2 \cdot 2H_2O$), ($NiCl_2 \cdot 6H_2O$), ($AgNO_3$), ($N_2H_4 \cdot H_2O$), PEG (biopolymer), PVP (synthetic polymer)	Wet chemical reduction method	Cu and Ag were spherical to cubic, uniform, and homogeneous in morphology, the Ni-NPs were polycrystalline 3–25 nm (Cu-NPs), 7–38 nm (Ni-NPs), and 4–45 nm (Ag-NPs)	Degradation of crystal violet, bromocresol green, and methylene blue	98
Ag NPs	*Peltophorum pterocarpum* leaves, NaOH pallets, $AgNO_3$, nitric acid	80 °C for 45 min at pH 9	Spheres and ellipses with sizes in the range of 2–50 nm	Degradation of methylene blue dye	104

the hydride and water for maritime and portable energy applications, which raises system complexity and lowers gravimetric efficiency.[92–96]

Sodium borohydride ($NaBH_4$) is one of the most effective reducing co-catalysts for dye degradation because of its high hydride-donating capacity and rapid electron-transfer kinetics. $NaBH_4$ facilitates the rapid and often complete reduction of a range of dye molecules under moderate reaction conditions when paired with suitable catalysts, such as metal nanoparticles or nanoclusters, leading to notable degradation efficiencies in short amounts of time. $NaBH_4$'s great reactivity makes it an excellent choice for laboratory-scale research and mechanistic investigations of catalytic dye degradation. On the other hand, alternative reducing agents like formic acid, sodium sulphite, sodium dithionite, and hydrazine hydrate usually exhibit slower reaction kinetics or lower reduction potentials, which may lead to lower degradation rates, the requirement for harsher operating conditions, and the generation of secondary byproducts.[97] Although these agents are often less expensive and may thus be more suitable for large-scale applications, their efficacy is limited by their inefficiency and compatibility with different catalytic systems. Economically speaking, $NaBH_4$'s somewhat higher cost would prohibit its direct use in large-scale wastewater treatment; however, this drawback is largely compensated for by its high efficiency, low dosage need, and effectiveness under ambient conditions. As a result, while less costly reducing agents are still being researched for economically viable industrial-scale applications, $NaBH_4$ is typically used in high-efficiency catalytic dye degradation experiments.[98,99]

7. Nanoparticles for dye degradation with $NaBH_4$ as a co-catalyst

$NaBH_4$ is an excellent reducing agent that turns metal salts like Ag^+, Au^{3+}, and Pd^{2+} into their metallic forms. This rapid reduction enables the controlled synthesis of uniform nanoparticles. $NaBH_4$ is a popular choice for making noble metal nanostructures for use in catalysis, sensing, and biomedical applications because it is efficient, selective, and works well with a range of solvents.[100,101]

In the review article we discussed Ag, Au, Fe, Cu and Ni nanoparticles as well as Ag nanoclusters, which were reported for the removal of dye with the help of $NaBH_4$. We also mentioned them in this regard in tabular form (Table 3, Fig. 2 and 3) in the following section.

The production of metal nanoparticles utilising various reducing and stabilising systems has been described using a variety of green and wet-chemical methods. Ferric chloride hexahydrate was used as the iron precursor in the green synthesis of iron nanoparticles (FeNPs), with Vernonia amygdalina leaf extract acting as a natural reducing and capping agent. Plant extract was added dropwise to the iron salt solution under ambient conditions, which facilitated fast nanoparticle production. To acquire pure FeNPs, centrifugation, washing, and air drying were then performed. Another study used polydopamine (PDA)-mediated surface functionalisation to

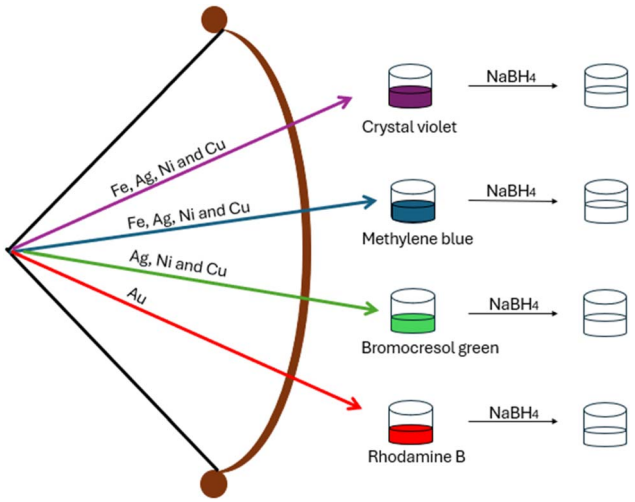

Fig. 2 This picture is a schematic diagram that shows how various metal nanoparticles contribute to the catalytic degradation of dyes with the help of $NaBH_4$. Each of the coloured arrows that emerge from the common source point on the left represents a catalyst for nanoparticles: the purple arrow indicates that Fe, Ag, Ni, and Cu nanoparticles are used to degrade crystal violet; the blue arrow indicates that Fe, Ag, Ni, and Cu are used to degrade methylene blue; the green arrow indicates that bromocresol green is degraded with Ag, Ni, and Cu; and the red arrow indicates that Au nanoparticles are used to degrade rhodamine B. On the right, each dye is shown as a coloured liquid in a beaker: rhodamine B (red), bromocresol green (green), methylene blue (blue), and crystal violet (purple). Arrows marked $NaBH_4$ point to nearby beakers, signifying reduction or degradation in the presence of sodium borohydride.

immobilise gold nanoparticles onto polyvinyl alcohol beads. In order to create a strong PVA-PDA@Au composite, PDA concurrently functioned as a stabilising and reducing agent, transforming Au^{3+} ions from chloroauric acid into metallic Au nanoparticles evenly attached on porous PVA beads. Hydrazine hydrate was used as a reducing agent in a modified wet-chemical reduction procedure to create metal nanoparticles of copper, nickel, and silver. Polyethene glycol and polyvinylpyrrolidone were used as stabilisers to avoid aggregation. The reaction was carried out at a high temperature in an alkaline environment to enable controlled reduction and nucleation. It was then purified and stored in an inert atmosphere to avoid oxidation. On the other hand, biomolecules from plant extracts such as *Imperata cylindrica* leaves and *Peltophorum pterocarpum* served as both capping and reducing agents in green production methods for silver nanoparticles. Efficient AgNP creation was made possible by optimising extract volume, pH, temperature, and reaction time. This was demonstrated by distinctive colour changes and verified by elemental analysis and post-synthesis purification. Together, these investigations show that stable metal nanoparticles may be produced using both chemical and green reduction techniques, with synthesis conditions being crucial in regulating particle formation, stability, and application.

An ecologically safe, economically feasible, and sustainable method of producing iron nanoparticles (FeNPs) is green synthesis, which uses plant extracts. This method eliminates the need for dangerous chemicals and intricate processing processes by using easily accessible plant-derived biomolecules in aqueous media that serve as both stabilising and reducing agents at the same time. In order to facilitate scalability and simplify operation, the synthesis is usually conducted under mild conditions, such as controlled stirring, light heating, and centrifugation. For large-scale applications, these limitations are usually acceptable, even if variations in phytochemical content may lead to batch-to-batch variations and restrict precise control over particle size and shape in comparison to conventional chemical approaches. Because stringent monodispersity is not a crucial criterion, plant-mediated synthesis is especially well suited for the large-scale manufacturing of FeNPs for wastewater treatment and environmental remediation, as mentioned in Table 4. On the other hand, because of their higher cost, increased chemical reactivity, and possible ecotoxicity, silver-based materials have substantial limits for widespread environmental deployment. Concerns about the

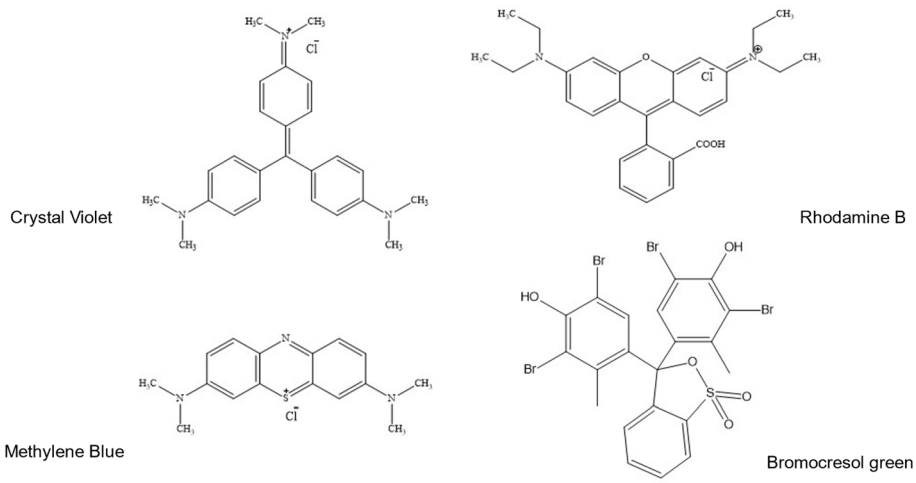

Fig. 3 The systematic diagram of atoms, functional groups, and conjugated systems makes up the molecular architecture of dye compounds.

Table 4 Various properties of metal nanoparticles with $NaBH_4$

Properties	Iron nanoparticles	Silver nanoparticles	Gold nanoparticles
Metal ion reduction	$Fe^{3+}/Fe^{2+} \rightarrow Fe^0$	$Ag^+ \rightarrow Ag^0$	$Au^{3+} \rightarrow Au^0$
Reduction kinetics	Very sensitive to reaction conditions; somewhat sluggish	Quick and effective; rate rises with concentration of $NaBH_4$	Due to Au^{3+}'s great reduction potential, it happens quite quickly
Role of $NaBH_4$ in dye degradation	Keeping the atmosphere reductive and providing electrons for the reduction of dyes	Provides electrons by surface-assisted oxidation; AgNPs effectively transfer electrons	Serves as a constant supply of electrons; AuNPs transfer electrons to dye molecules
e^- Transfer mechanism	FeNPs serve as less effective electron relay hubs	AgNPs facilitate quick electron transfer, which is amplified by plasmonic effects	AuNPs serve as mediators and stable electron stores
Concentration of $NaBH_4$	Aids in reducing oxidation, but is unable to completely stop instability	Can result in borate aggregation or surface blockage	Generally steady, minimal negative impact

usage of silver in large freshwater or marine systems are raised by the fact that high quantities of the metal can be harmful to aquatic life. Due to their lower reactivity, which minimises uncontrolled ion release and lowers the potential of secondary contamination in vast aquatic ecosystems, iron-based materials are a more feasible option with greater abundance, affordability, and environmental compatibility.[105,106]

The interconnected nucleation, growth, reduction kinetics, and stability mechanisms that control nanoparticle formation in $NaBH_4$-assisted systems are extremely sensitive to reaction conditions and metal identity. $NaBH_4$ concentration plays a crucial role in regulating metal atom supersaturation during the initial nucleation and growth stages of particle growth. Lower concentrations encourage slower nucleation and longer growth, resulting in larger and frequently aggregated particles, while higher concentrations cause rapid burst nucleation, resulting in smaller and more evenly distributed nanoparticles. Temperature controls atomic mobility and reduction kinetics, reaction time dictates the degree of Ostwald ripening, and pH affects BH_4^- stability and nanoparticle surface charge, which in turn affects aggregation and dispersion. In order to stop uncontrollable aggregation, stabilisers further modify surface energy. Concurrently, the rate at which metal ions (such as Ag^+, Au^{3+}, Pd^{2+}, and Fe^{3+}) are transformed into their metallic states is determined by reduction kinetics, with $NaBH_4$ serving as a hydride and electron source. While conductive and plasmonic metals promote more effective interfacial electron transport, metals with higher standard reduction potentials, such Au and Ag, show quicker reduction rates than Fe-based systems. Time-resolved spectroscopic and kinetic investigations show that metal-dependent reduction behaviour is further influenced by variations in coordination chemistry, ion hydration, and electronic structure. Particularly under aqueous and repetitive catalytic conditions, the resulting nanoparticles' long-term stability is determined by their susceptibility to oxidation, aggregation, borate-induced surface passivation, and metal leaching. Fe-based systems are more vulnerable to oxidation, while Ag- and Pd-based systems are more vulnerable to aggregation or surface blocking at high $NaBH_4$ concentrations. Crucially, these mechanistic pathways are highly reaction–condition specific; variations in $NaBH_4$ concentration, pH, reaction duration, and metal type result in noticeably different kinetic and stability outcomes, requiring condition-dependent and metal-specific analyses instead of broad interpretations. Therefore, in order to enable rational catalyst design rather than descriptive trend reporting, a core-level debate necessitates mechanistic cause-and-effect correlations connecting synthesis conditions to nucleation behaviour, reduction rates, electronic structure, and surface chemistry. To prevent speculative conclusions, such interpretations must be carefully backed by peer-reviewed evidence, such as kinetic constants, spectroscopic analysis, and microscopic characterisation. The review's scientific rigour, practical relevance, and wider appeal to researchers interested in catalyst design, scalability, and environmental applications are all improved by including this depth of mechanistic insight, which turns it from a narrative overview into a predictive framework.[97,107,108]

7.1 Evolution of nanoparticles

Green production of iron nanoparticles (FeNPs) was reported by the authors of ref. 69 using a modified approach based on a known technique.[109–111] Iron was derived from ferric chloride hexahydrate ($FeCl_3 \cdot 6H_2O$). 75 mL of 0.1 M $FeCl_3 \cdot 6H_2O$ solution was continuously stirred with a magnetic stirrer at room temperature while an equal volume (75 mL) of *Vernonia amygdalina* leaf extract was added dropwise. A distinctive greyish-black colouring appeared after around five minutes, indicating the synthesis of FeNPs. To recover the nanoparticles, they were centrifuged for 15 minutes at 5000 rpm to eliminate unreacted precursors and contaminants. This was followed by three consecutive washings with ethanol and distilled water. At room temperature, the purified FeNPs were then allowed to air dry before being placed in airtight containers for use in later processes.[69] Polyvinyl alcohol (PVA) beads coated with gold nanoparticles (AuNP) were created by a multi-step process. The first step was to dissolve sodium alginate (SA), PVA, and calcium carbonate ($CaCO_3$) in deionised water and stir constantly for four hours at 95 °C to create a homogeneous mixture. Ionic crosslinking enabled the creation of beads after the solution was cooled and extruded into a boric acid solution that was saturated with calcium chloride ($CaCl_2$). The resultant beads were left for 48 hours to harden. The $CaCO_3$ template particles

were dissolved by hydrochloric acid (HCl), which was applied to the hardened beads to provide porosity. The porous beads were then kept in an aqueous solution after being carefully cleaned with deionised water. Polydopamine (PDA) was applied to the PVA beads for surface functionalisation by dispersing them in Tris–HCl solution (pH 8.5) containing dopamine hydrochloride and stirring for six hours. This allowed the dopamine to undergo oxidative self-polymerization and generate a consistent layer of PDA on the bead surface. The PDA-coated beads were incubated for 12 hours in an aqueous solution of chloroauric acid ($HAuCl_4$) in order to load AuNPs. PDA's catechol and amine groups served as stabilising and reducing agents, turning Au^{3+} into metallic Au^0 nanoparticles that were immobilised on the surface of the bead. The composite that was produced was called PVA-PDA@Au beads. PVA beads, PDA-functionalized PVA beads (PVA-PDA), and colloidal AuNPs were all synthesised separately under comparable conditions for comparative analysis. Reported by the authors of ref. 102, M-NPs (copper, nickel, and silver metal nanoparticles) are created using a modified wet chemical reduction technique.[112] Polyethylene glycol (PEG) and polyvinylpyrrolidone (PVP) were used as stabilisers to improve nanoparticle stability and avoid aggregation, while hydrazine hydrate served as the reducing agent in this procedure. Copper(II) chloride dihydrate ($CuCl_2 \cdot 2H_2O$), nickel(II) chloride hexahydrate ($NiCl_2 \cdot 6H_2O$), and silver nitrate ($AgNO_3$) were the metal precursors used. 0.350 g of the selected metal salt and 0.250 g of the stabilising polymer were ultrasonically dispersed in a binary solvent solution consisting of equal quantities (50 mL each) of anhydrous ethanol and ethylene glycol for the synthesis. The precursors and stabilisers interacted effectively and were mixed uniformly thanks to ultrasonication. After that, sodium hydroxide (NaOH) was used to bring the solution's pH down to 12, which produced an alkaline environment that was ideal for reduction. To control the reduction kinetics and nanoparticle nucleation, a reducing solution made of hydrazine hydrate (8 mL mixed in 10 mL ethanol) was then introduced progressively in a dropwise fashion. For four hours, the reaction mixture was kept at 80 °C while being constantly stirred to enable the full reduction of metal ions to their equivalent zero-valent nanoparticles. The system was allowed to cool to room temperature when the reaction was completed. Following centrifugation, the nanoparticles were extensively cleaned with ethanol to get rid of any remaining precursors and stabilisers and then allowed to air dry. In order to safeguard their structural integrity and avoid oxidation, the refined nanoparticles were lastly kept in airtight containers that had been nitrogen-purged as reported by the authors of ref. 113. The first step in the ecologically friendly green synthesis of silver nanoparticles (AgNPs) was optimisation to identify the best synthesis conditions. *Peltophorum pterocarpum* leaf extract (PPLE) volume, pH, temperature, and reaction time were among the variables that had to be changed. Ultimately, the optimised synthesis was conducted at 80 °C using 200 mL of PPLE and 40 mL of 1 mM $AgNO_3$, while keeping the volume ratio at 20 : 4. With the use of 0.1 M NaOH, the pH was brought to 9. The reaction mixture was maintained for forty-five minutes at 80 °C. To get rid of any unreacted metal precursors, the dark brown product was recovered by centrifugation at 10 000 rpm for 30 minutes and then washed with distilled water. As necessary, this cleaning process was repeated. To guarantee a homogeneous dispersion, the final product volume was set at 200 mL and sonicated. Following microwave digestion with 69% nitric acid, the amount of silver in the solution was measured using Inductively Coupled Plasma Optical Emission Spectroscopy (ICP-OES).[104] *Imperata cylindrica* leaves were gathered from a specific location at the Technology University MARA in Shah Alam, Selangor, Malaysia. After being carefully cleaned with distilled water, the leaves were oven-dried for 48 hours at 60 °C. A regular food processor was used to grind them into a fine powder once they had dried. 5 g of the powdered leaves were combined with 200 millilitres of distilled water, agitated, and boiled for thirty minutes at 60 °C to create the aqueous leaf extract. The plant residue and extract were separated by filtering the resultant combination. 90 mL of a 5 mM aqueous silver nitrate ($AgNO_3$) solution was mixed with 10 mL of the obtained extract to create silver nanoparticles (AgNPs). For ten minutes, this mixture was heated to 60 °C in a water bath. The solution started to become brown, which was a sign that silver nanoparticles were forming (Fig. 4).[103]

7.2 Degradation of dyes by using synthesised nanoparticles with $NaBH_4$

The use of biosynthesised iron nanoparticles (FeNPs) for the catalytic degradation of organic dyes was studied by the authors of ref. 69. As a reducing agent, sodium borohydride ($NaBH_4$) was added to methylene blue (MB) and crystal violet (CV) aqueous solutions to start the degradation process. Following that, the reaction mixture was supplemented with an optimal dose of FeNPs. The dye solution, $NaBH_4$, and FeNPs were mixed and continuously stirred magnetically to guarantee that the reactants interacted uniformly. Following the specified reaction time, the suspension was centrifuged for five minutes at 1500 rpm in order to minimise nanoparticle dispersion and help separate FeNPs from the treated dye solution. Using spectrophotometry, the absorbance of the solutions at their respective maximum absorption wavelengths, 590 nm for CV and 664 nm for MB, before and after treatment, was measured to determine the degree of dye degradation. At these wavelengths, a decrease in absorbance intensity verified FeNPs' catalytic activity in accelerating dye degradation mediated by $NaBH_4$.[69]

$$\text{Degradation percentage} = \frac{A_0 - A_t}{A_0} \times 100 \quad (3)$$

Using various materials, the authors of ref. 102 conducted a comparative analysis of Rhodamine B (RhB) catalytic degradation. After 60 minutes, the removal effectiveness of pure gold nanoparticles (AuNPs) was 11.3%, but the adsorption capabilities of polyvinyl alcohol (PVA) and polydopamine-modified PVA (PVA-PDA) beads alone were only 5.0% and 5.9%, respectively. But the degradation efficiency rose dramatically to 98.4% when sodium borohydride ($NaBH_4$) was present. Using PVA-PDA@Au

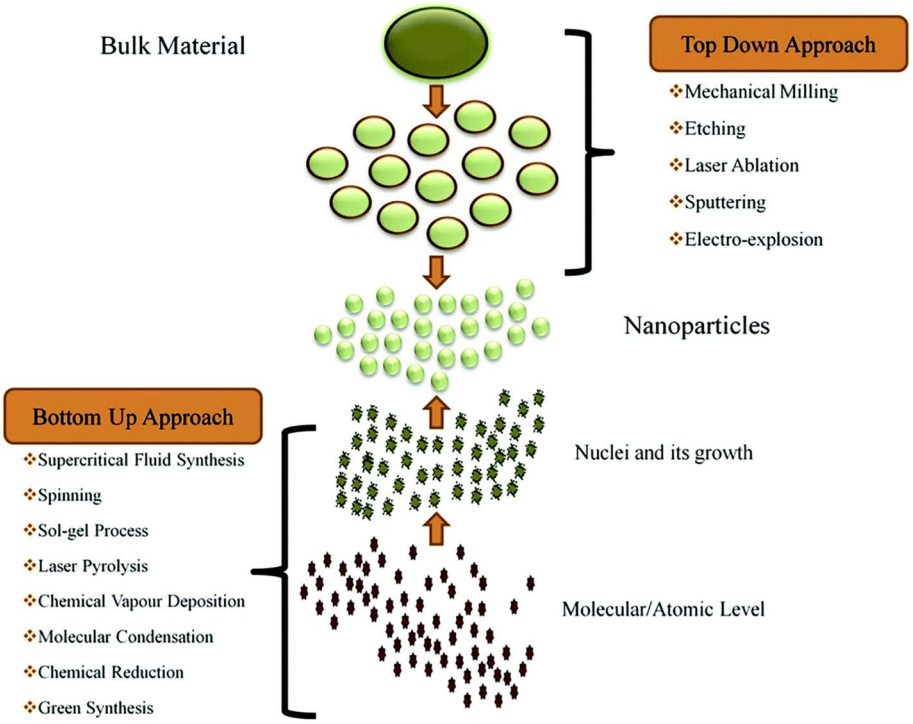

Fig. 4 The two primary methods for producing nanomaterials depend on how the material is constructed or degraded, adapted/reproduced from ref. 110 with permission from Elsevier [*J. Microbiol. Methods*], copyright 2019.

beads resulted in a dramatic improvement, with ~99.5% degradation seen in just 5 minutes and total removal >100% after 60 minutes. The PDA coating's stabilisation of AuNPs, which inhibits nanoparticle aggregation, improves dye adsorption, and promotes more effective electron transfer during the catalytic process, is responsible for the composite beads' better performance. On the other hand, because of aggregation brought on by their high surface energy, which decreased the number of available active sites, unsupported AuNPs showed poorer catalytic activity. This demonstrates how important the PVA-PDA support is for enhancing AuNP stability and catalytic performance for efficient dye degradation.

$$\text{Removal efficiency}(\%) = \frac{C_0 - C_t}{C_0} \times 100 \quad (4)$$

Three typical dyes were used to evaluate the synthesised metal nanoparticles' (M-NPs') catalytic capability. At a starting dye concentration of 1 mM, almost 80% of the anionic dyes, crystal violet (CV) and bromocresol green (BCG), were broken down in 90–120 minutes. By contrast, the cationic dye methylene blue (MB) degraded 80% faster, in 30 to 60 minutes. In its oxidised state, the water-soluble thiazine dye methylene blue has a distinctive absorption maximum at 665 nm. It changes into its colourless reduced form, leuco-methylene blue (LMB), when exposed to reducing chemicals such as sodium borohydride ($NaBH_4$). Even after 24 hours without outside assistance, treating MB solutions with 2% (w/v) $NaBH_4$ alone caused less than 5% discolouration. On the other hand, the addition of M-NPs to the $NaBH_4$-MB system significantly sped up the reaction, resulting in almost total decolourisation in just four hours. Despite being a potent reducing agent, $NaBH_4$ is not very successful in degrading dyes in ambient environments, where light energy is essential for improving reaction kinetics. This observation is in line with the results of Ayodhya and Veerabhadram, who showed that CdS nanoparticles in the presence of $NaBH_4$ obtained a degradation efficiency of 97% for MB under light irradiation, but the efficiency dropped to less than 50% under dark conditions.[114–116] By monitoring the chemical breakdown of methylene blue (MB) dye using a UV-vis spectrophotometer, the catalytic effectiveness of the biosynthesised AgNPs was evaluated. Without a catalyst, the breakdown happened gradually. Nevertheless, the addition of AgNPs considerably sped up the reaction and shortened its duration. Over time, there was a noticeable drop in absorbance at 665 nm, the main peak linked to MB dye. A high pseudo-first-order rate constant of 0.3378 min^{-1} was observed along with 82% degradation in 6 minutes at an ideal pH of 7.5. As the catalyst surface got saturated with the product, further degradation was restricted after this. Only 44% degradation was attained after 16 minutes, and the reaction rate drastically decreased under acidic conditions (pH 3), with a much lower rate constant of 0.0383 min^{-1}. The high proton concentration, which prevents the cationic dye from interacting with the AgNP surface, is the cause of this decrease. Although 81% degradation was seen in 8 minutes at an alkaline pH of 10, the interaction between BH_4^- and the catalyst surface was probably hampered by the increased presence of OH^-. Therefore, the most effective pH

was neutral. The deterioration process was further accelerated by raising the temperature to 70 °C, reaching 90% degradation in just 2.5 minutes. This was probably caused by more molecular collisions and energy. With just 16% degradation after 18 minutes, the degradation efficiency drastically decreased when the amount of MB dye was raised fivefold. This suggests that the AgNPs have saturated the surface, which restricts the reducing agent's ability to reach the dye molecules. The development of leucoMB, a less hazardous version of the dye, was indicated by a noticeable colour shift from blue to colourless at pH 7.5, pH 10, and higher temperatures. AgNPs mediate the electron transfer from $NaBH_4$ to MB dye, which is the degradation process. AgNPs offer an electron-rich surface that facilitates the contact. Furthermore, through hydrophobic interactions and van der Waals forces, phytochemicals stabilising the AgNPs may improve dye adsorption onto the nanoparticle surface. In general, the authors of ref. 103,104 indicated that the AgNPs showed catalytic performance similar to other plant-extract-mediated AgNPs. In the presence of sodium borohydride ($NaBH_4$), biosynthesised silver nanoparticles (AgNPs) showed promise as catalysts in the reduction of methylene blue (MB) to its colourless form, leuco methylene blue (LMB). As electron mediators, the AgNPs help the reduction reaction by transferring electrons from the BH_4^- ions, which act as donors, to the dye molecules, which act as electron acceptors. Because the BH_4^- ions adhere to the nanoparticles' surface, electrons can go from the donor to the dye *via* the nanoparticles. MB has a significant absorption peak at 664 nm and a secondary peak at 615 nm in aqueous solution. At room temperature, the reduction process was monitored using UV-visible spectroscopy in the 300–900 nm region. Dye degradation was demonstrated by a progressive drop in absorbance at 664 nm over time. The MB solution's bright blue hue gradually diminished as the reaction went on, eventually turning colourless. To track the development of the reaction, the dye concentration at time t (C) was compared to its initial concentration (C_0). With degradation ranging from just 1.02% to 2.61%, the decrease of MB in the absence of the biosynthesised AgNPs was negligible. But once the AgNPs were added, the process was greatly accelerated, reaching up to 92.06% degradation in just 14 minutes (Fig. 5).[103,117]

The comparison of research on dye degradation using nanoparticles reveals distinct variations and parallels in the selection of nanomaterials, production methods, reaction processes, and functional performance. According to the authors of ref. 69, iron nanoparticles made using a sustainable method using *Vernonia amygdalina* leaf extract were used. The FeNPs served as a catalyst and reductant without the need for sodium borohydride. Catalytic reduction and surface-mediated electron transfer were the primary methods of dye removal in this system, providing an ecologically safe method with high catalytic efficiency. However, mild stability problems associated with oxidation and aggregation were noted. The authors of ref. 102, on the other hand, created a chemically designed catalyst by depositing gold nanoparticles on PVA beads functionalised with polydopamine. In this system, AuNPs served as electron-shuttling centres while $NaBH_4$ played a critical function as a hydride and electron donor. This led to effective catalytic reduction of organic dyes and high stability and recyclability because of the solid bead support. $NaBH_4$ was not specifically used in ref. 103 for the synthesis of silver nanoparticles for methylene blue degradation using *Imperata cylindrica* aqueous extract. Adsorption and surface catalytic activity of colloidal AgNPs dominated the degradation pathway, allowing for

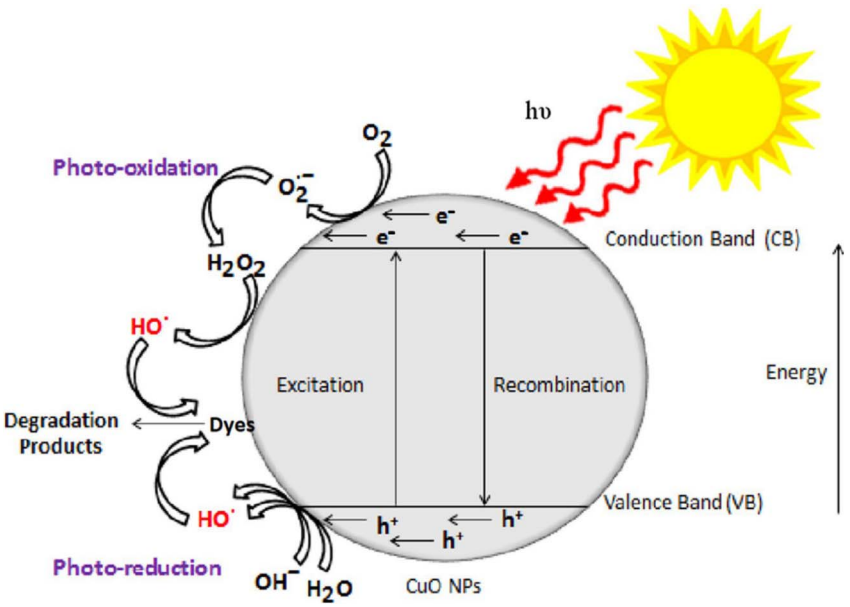

Fig. 5 A schematic representation of photocatalytic dye degradation shows that the main reactive species that break down dyes in aqueous solutions are hydroxyl radicals (•OH) and voids in the catalyst structure, adapted/reproduced from ref. 118 with permission from MDPI [*Catalysts*], copyright 2023.

a straightforward and inexpensive method with minimal recyclability. The authors of ref. 98 provided a thorough analysis of green photocatalytic nanomaterials for the degradation of various dyes, mostly systems based on silver. $NaBH_4$ was only considered in a broad catalytic framework rather than as a fundamental reactant in their work, which focused on light-driven photocatalytic pathways involving reactive oxygen species, including hydroxyl and superoxide radicals. Ogundare *et al.*[104] reported green-synthesised AgNPs using *Peltophorum pterocarpum* leaf extract, where biological capping agents improved durability while adding extra antibacterial functionality, and dye degradation proceeded through catalytic reduction on the AgNP surface without $NaBH_4$.

7.2.1 Mechanism of sodium borohydride-induced dye degradation with nanocatalysts

7.2.1.1 General mechanism. Silver nanoparticles (AgNPs) function as extremely effective electron mediators because of their high electrical conductivity and advantageous Fermi level alignment. BH_4^- ions undergo surface-assisted oxidation to borate species upon adsorption of $NaBH_4$, releasing electrons that are quickly moved to nearby dye molecules adsorbed on the AgNP surface. By reducing non-radiative energy losses and reducing fluorescence quenching, Ag^+ (or Ag_2) clusters' d^1 electronic structure promotes efficient charge transfer. AgNPs therefore encourage the quick reduction of chromophoric moieties, especially conjugated aromatic and azo groups.[98]

$NaBH_4$ acts as an electron donor in catalytic systems based on gold nanoparticles (AuNPs), effectively transferring electrons across the highly conductive and chemically durable gold surface. AuNPs and BH_4^- ions have a strong connection that minimises nanoparticle oxidation and aggregation while promoting efficient electron donation. AuNPs sustain catalytic activity across several reaction cycles due to their intrinsic surface stability. A Langmuir–Hinshelwood process, in which $NaBH_4$ and the substrate molecules are co-adsorbed onto the AuNP surface before the reduction reaction, is primarily responsible for electron transport.[119]

Iron nanoparticles (FeNPs) have dual roles as redox-active catalysts and electron mediators. By acting as an electron and hydride donor, sodium borohydride ($NaBH_4$) reduces surface Fe^{3+}/Fe^{2+} species to Fe^0, regenerating catalytically active sites. However, electron transport may be gradually hampered by partial surface oxidation of FeNPs. $NaBH_4$ is therefore essential for preserving the reduced state of the iron surface, avoiding passivation, and ensuring a steady flow of electrons to dye molecules that have been adsorbed.[69,120]

$NaBH_4$ continually reduces surface Cu^{2+}/Cu^+ species produced throughout the reaction, stabilising Cu_2 in copper nanoparticle (CuNP)-based catalytic systems. Although surface copper atoms facilitate electron transmission, CuNPs are more vulnerable to surface oxidation than noble metal nanoparticles. As a result, $NaBH_4$ serves as a stabilising agent that lessens catalyst deactivation as well as an electron donor for substrate reduction.[121]

$NaBH_4$ does not directly degrade dye molecules in the homogeneous solution phase across all metal nanoparticle systems. Instead, the nanoparticles serve as electron-transfer mediators that decrease the activation energy and improve reduction kinetics, and it serves as a co-catalyst and electron reservoir. The electrical structure, redox stability, and resistance to surface passivation of the metal nanoparticle substantially influence the effectiveness of $NaBH_4$-assisted electron transfer.

In dye degradation mediated by nanoparticles, $NaBH_4$ is an essential co-catalyst because it stabilises the catalytic surface and provides a steady supply of electrons. $NaBH_4$ dissociates in aqueous environments to produce BH_4^- ions. These ions easily adsorb onto the surface of metal nanoparticles like Ag, Au, Cu, or Fe, placing the reducing species near catalytically active locations. BH_4^- undergoes surface-assisted oxidation to borate species upon adsorption, releasing electrons that are then injected into the conduction band or surface of the nanoparticle. In order to effectively reduce important chromophoric functionalities, such as azo (–N=N–), nitro ($–NO_2$), and conjugated aromatic groups, these electrons are then transferred through the nanoparticle to dye molecules co-adsorbed on the surface *via* a Langmuir–Hinshelwood-type mechanism.[122] This ultimately results in dye decolourisation and molecular breakdown. By continuously reducing oxidised surface species (Fe^{3+}/Fe^{2+} or Cu^{2+}/Cu^+) back to their zero-valent states, $NaBH_4$ further plays a crucial role in sustaining catalytic activity in systems using transition metal nanoparticles like Fe and Cu. This prevents surface passivation and loss of conductivity. $NaBH_4$ maintains constant electron flow, maintains the catalyst's active metallic state, and permits effective and reproducible dye degradation across several catalytic cycles by acting as both an electron donor and a surface stabiliser.[69,120]

$$\mathrm{Dye_{(aqu)} + BH_4^- \xrightarrow{NPs(surface\ adsorption)} [dye, cdotpNP, cdotpBH_4^-]adsorbed}$$

$$\mathrm{BH_4^- \xrightarrow{NP\ surface} BH_3 + H^-(electron\ donor)}$$

$$\mathrm{Dye^+ + e^- \rightarrow Leuco\ dye\ (reduced\ form)}$$

$$\mathrm{MB(blue,\ oxidized) + BH_4^- \xrightarrow{NP\ catalyst} Leuco\ MB(colourless) + byproducts(BH_3, H_2O)}$$

7.2.1.2 Selective mechanism. Aroob *et al.*[118] reported green chemically synthesized CuO nanoparticles for the degradation of industrial dyes with $NaBH_4$ as a co-catalyst. The main reactive species in charge of dye detoxification are identified through an examination of the photocatalytic process under solar radiation, which also makes it possible to develop a tenable degradation mechanism. Because relatively low photon energy is sufficient to facilitate electronic transitions from the valence band to the conduction band, or from the highest occupied molecular orbital (HOMO) to the lowest unoccupied molecular orbital (LUMO), nanomaterials with a narrow band gap easily absorb incident light. Conduction band electrons ($e_{(CB)}^-$) and

equivalent valence band holes ($h_{(VB)}^{+}$) are produced when light is absorbed and electrons are excited from the ground state to the excited state. At the catalyst surface, these photogenerated charge carriers are essential to redox processes. Because of their great oxidising potential, the valence band holes can either directly oxidise adsorbed dye molecules or react with surface-adsorbed water or hydroxide ions to form highly reactive hydroxyl radicals ($^{\bullet}OH$), which can break down organic pollutants. Superoxide radicals ($O_2^{\bullet -}$) are created when the conduction band electrons simultaneously decrease dissolved molecular oxygen. These radicals then take part in subsequent oxidation events that break down and mineralise colour molecules.[123]

7.3 Effect of sodium borohydride's different concentrations

By providing a higher density of borohydride ions (BH_4^-), which serve as efficient electron donors to the electron-deficient dye molecules, an increase in sodium borohydride ($NaBH_4$) concentration considerably accelerates the rate of dye breakdown. Increased adsorption of BH_4^- ions onto the nanoparticle surface is also encouraged by elevated $NaBH_4$ concentrations, which enhances the efficiency of electron transfer at the catalyst–dye interface. In other words, direct correlation as well as adsorption effects facilitated the process of dye removal with the increase of $NaBH_4$ concentration. Even though $NaBH_4$ is essential to the reaction process, an overly high dosage can negatively impact system performance by causing the catalytic nanomaterials to become structurally unstable, increasing charge-carrier recombination losses, and producing light-shielding effects that lower effective photon absorption.[69,97]

In 2024, Jara *et al.*[69] found that the degradation efficiency increased with increasing $NaBH_4$ concentration from 0.01 M to 0.12 M, with 0.12 M showing the best performance. This figure was determined to be the ideal concentration, highlighting how crucial it is to maintain a suitable BH_4^- ion level for efficient degradation aided by nanoparticles. Furthermore, the higher concentration of $NaBH_4$ raised the electron density on the FeNPs' surface, which probably accelerated the pace of reaction. Zhang, Z. & Wu Y. in 2010 performed an experiment in which different concentrations of $NaBH_4$ were used to aggregate gold nanoparticles and found that different concentrations can form different size nanoparticles.[124]

7.4 Kinetic study

Kinetic analysis is a technique used to examine how quickly a dye decolorises when exposed to an oxidant, reductant, or catalyst (such as metal nanoparticles). Under some conditions, it aids in determining the rate constants, the sequence of the reaction, and the pace at which it proceeds. When a reaction's rate doesn't change over time and is independent of the reactant's concentration, it seems to follow zero-order kinetics. When there is a significant excess of one reactant in a reaction involving two, the concentration of that reactant essentially remains constant, reducing the kinetics to first order with regard to the limiting reactant (Table 5 and Fig. 6).

$$C_0 - C = k_0 t \tag{5}$$

$$\ln \frac{C_0}{C_t} = k_0 t \tag{6}$$

$$\frac{1}{C} - \frac{1}{C_0} = k_2 t \tag{7}$$

where C = concentration, k = rate constant, and t = time.

7.4.1 Pseudo zero-order analysis. The degradation of two dyes, crystal violet and methylene blue, by iron nanoparticles (FeNPs) was analyzed. To comprehend the response behaviour, they used various kinetic models to analyse the degradation. For both dyes, they discovered that the pseudo-zero-order kinetic model offered the greatest match. This indicates that, independent of the dye's concentration in solution, the rate of dye degradation was consistent throughout time. Very high $R2$ values (around 1) supported this conclusion: for methylene blue, 0.999; for crystal violet, 0.995. These strong correlation values ($R2$) demonstrate how well the experimental data matched the zero-order model's predictions.[69]

7.4.2 Pseudo first order analysis. Only the catalytic breakdown of methylene blue has a comparatively high correlation coefficient, according to pseudo-first-order kinetics. These results indicate that the catalytic degradation process on the FeNP catalyst surface follows pseudo-first-order kinetics, in

Table 5 Order and kinetics of dye degradation with $NaBH_4$ as a co-catalyst

Order	Catalyst	Co-catalyst	Dyes	Rate constant (k)	References
Pseudo zero order	Iron nanoparticles	$NaBH_4$	Methylene blue	0.088	69
	Iron nanoparticles	$NaBH_4$	Crystal violet	0.084	69
Pseudo first order	Iron nanoparticles	$NaBH_4$	Methylene blue	0.051	69
	Silver nanoparticles			0.0304 s^{-1}	125
	Silver nanoparticles			0.3378 min^{-1}	104
	Iron nanoparticles	$NaBH_4$	Crystal violet	0.041	69
	Silver nanoparticles	$NaBH_4$	Bromocresol green		113
	Silver nanoparticles	$NaBH_4$	Rhodamine B	0.0127 s^{-1}	125
	Silver nanoparticles	$NaBH_4$	Methyl orange	0.0179 s^{-1}	125
	Silver nanoparticles	$NaBH_4$	Congo red	0.0051 s^{-1}	125
Pseudo second order	Iron nanoparticles	$NaBH_4$	Methylene blue	0.033	69
	Iron nanoparticles	$NaBH_4$	Crystal violet	0.021	69

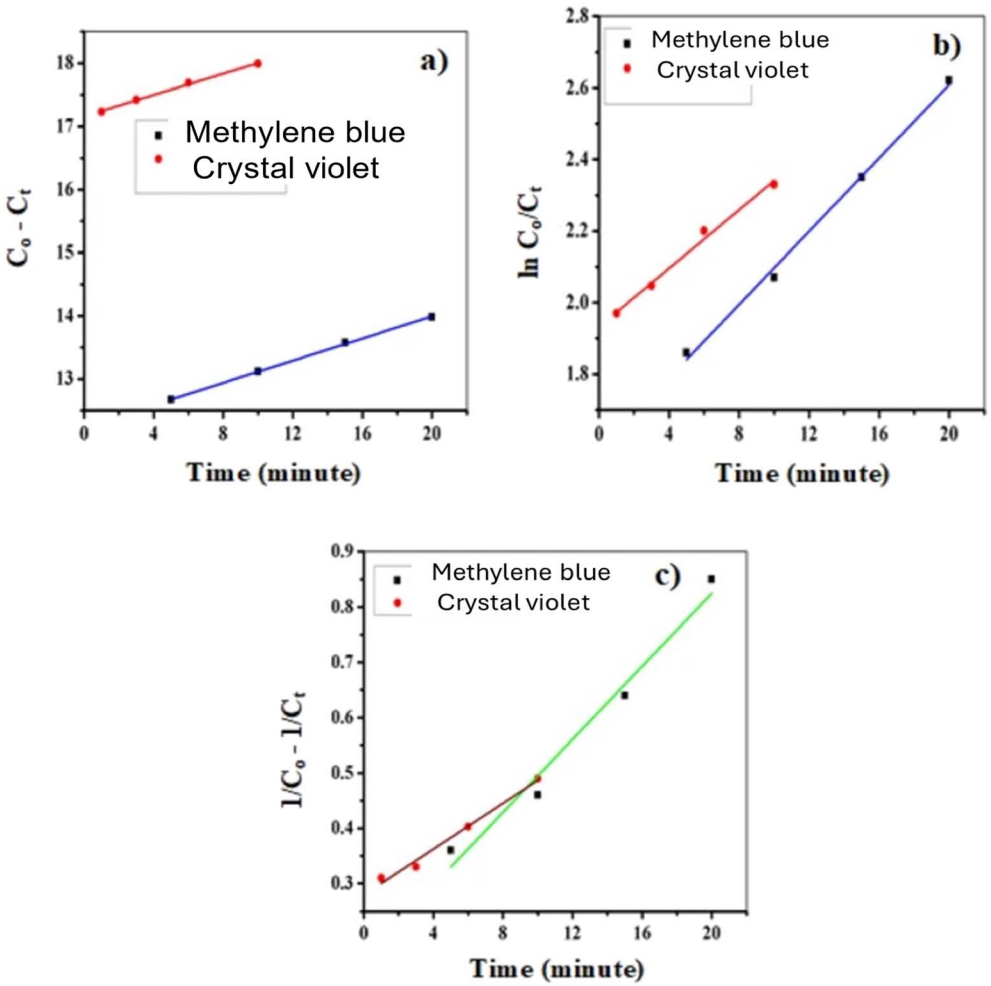

Fig. 6 Pseudo zero-order (a), pseudo first-order (b), and pseudo second-order (c) kinetic models were used to assess the reaction kinetics of iron nanoparticles' (FeNPs) catalytic degradation of crystal violet (CV) and methylene blue (MB) dyes in the presence of sodium borohydride ($NaBH_4$). These models correlate the change in dye concentration over time with the activity of the catalyst, which helps clarify the rate and process of dye degradation. The pseudo first-order model establishes a surface-limited process by linking the reaction rate to the concentration of a single reactant, usually the dye, while the pseudo zero-order model assumes that the degradation rate is independent of the original dye concentration. However, the pseudo second-order model, on the other hand, suggests adsorption-controlled kinetics by considering the reaction rate to be proportional to the square of the dye concentration or the contact between two reactants. The best reaction pathway controlling the catalytic activity of FeNPs during $NaBH_4$ assisted dye reduction can be found by comparing the experimental data with these kinetic models, adapted/reproduced from ref. 69 with permission from Springer Nature [*Scientific Reports*], copyright 2024.

which the dye concentration and catalytic degradation rate are directly proportional. Pseudo-zero-order kinetics was also suitable.[69] Three widely used dyes were utilised to test the synthesised metal nanoparticles' (M-NPs') catalytic efficacy in dye removal. About 80% of the anionic dyes, crystal violet (CV) and bromocresol green (BCG), were decolorised in 90 to 120 minutes at an initial dye concentration of 1 mM. The cationic dye methylene blue (MB), on the other hand, degraded more quickly with about 80% of it being decolorised in just 30 to 60 minutes. In its oxidised condition, MB, a water-soluble thiazine-based cationic dye, usually shows a prominent absorption peak at 665 nm. It transforms into leuco-methylene blue (LMB), a colourless form, when exposed to reducing chemicals such sodium borohydride ($NaBH_4$). Even after 24 hours, it was found that treating dye solutions with 2% (w/v) $NaBH_4$ alone caused less than 5% decolorisation. On the other hand, M-NPs caused almost total decolourisation in just four hours when added to dye solutions treated with $NaBH_4$. Under environmental conditions, light energy is essential for the degradation of dye pollutants, even if $NaBH_4$ functions as a reductant. According to the authors of ref. 114, methylene blue degradation with $NaBH_4$ and CdS nanoparticles under light irradiation reached 97%, as opposed to less than 50% without light. This finding supports this observation.[114,126–128] The catalytic activity of the biosynthesised silver nanoparticles (AgNPs) in breaking down the methylene blue (MB) dye was assessed using $NaBH_4$ as a reducing agent. Using UV-vis spectroscopy, the reaction was observed, namely the absorbance at 665 nm. Degradation proceeded according to pseudo-first-order kinetics. Compared to $NaBH_4$ alone, the AgNPs greatly accelerated the pace of the

reaction, attaining 82% degradation in 6 minutes at pH 7.5 and a high rate constant of 0.3378 min^{-1}. The pace and amount of degradation were decreased by acidic conditions (pH 3) (44% in 16 minutes), but alkaline conditions (pH 10) caused 81% disintegration in 8 minutes. Balanced surface charge interactions led to optimal performance at neutral pH. By raising the temperature to 70 °C, the process was further accelerated, reaching 90% degradation in just 2.5 minutes. The reaction was significantly slowed down by a five-fold increase in MB concentration, demonstrating AgNP surface saturation. The development of leuco-methylene blue was verified by a discernible colour shift from blue to colourless. AgNPs' electron-rich surface helped to transport electrons from $NaBH_4$ to MB. Additionally, through hydrophobic and van der Waals interactions, phytochemicals derived from plants stabilised the AgNPs and enhanced dye adsorption. For five cycles, the AgNPs were stable and catalytically effective, and HRTEM showed no discernible morphological alterations.[104]

7.4.3 Pseudo second order. The correlation coefficient of the pseudo-second-order model is lower for both dyes than that of other pseudo-kinetic models, including pseudo zero-order and pseudo-first-order models. This suggests that the pseudo-second-order model is not supported by the catalytic degradation of both dyes. Overall, the strong correlation value indicated that the zero-order pseudo kinetic model is a good fit for explaining how FeNPs break down both dyes. This discovery is significant because it suggests that FeNPs may be employed as efficient catalysts to break down these dyes in wastewater.[69]

7.5 Recyclability study of catalysts

Reusable catalysts are essential for effective and sustainable water treatment. By increasing turnover frequency and decreasing waste, reusable catalysts enhance process scalability and are consistent with the principles of green chemistry. Potential problems like metal leaching, agglomeration, or deactivation are revealed by evaluating reusability. Effective reuse reduces operating costs and promotes long-term environmental and economic viability in large-scale remediation for expensive metal nanoparticles (such as AgNPs, AuNPs, and PdNPs).[129,130] The reusability of the catalyst was examined during the degradation process under the same experimental settings (at the optimal concentration of dye solution, reducing agent, catalyst dosage, and duration), according to Jara and their team. Following the reaction's conclusion, the catalyst was centrifuged out of the reaction mixture, cleaned with water and ethanol, dried, and then used again for the second, third and fourth times in a row. The authors of ref. 69,102 convey that when evaluating PVA-PDA@Au beads' catalytic efficacy for wastewater treatment, two important factors were their structural stability and reusability. The beads were put through multiple RhB decolourisation procedures using the same catalyst in order to assess their recyclability. Following each cycle, the beads were collected using basic filtering, cleaned with water, and then put to further use. Throughout six consecutive cycles, the PVA-PDA@Au beads continuously demonstrated a high removal efficiency of over 99%, indicating exceptional stability and reusability. Furthermore, because the diffraction patterns closely matched those of the fresh sample, XRD examination demonstrated significant structural resilience and proved that the reused beads' structural integrity had not been compromised.[102] Yang *et al.* (2014)[130] found that stability and reusability of the catalyst are essential for realistic and expandable applications. In order to evaluate these parameters, the catalytic reduction processes were conducted again using a catalyst of 0.01 M $Cu(NO_3)_2$ under ambient conditions. The catalyst's durability and efficiency were proved by its steady performance over five consecutive cycles, maintaining a conversion efficiency exceeding 95%. According to UV-visible spectroscopic examination, catalytic activity only slightly decreased in the fifth cycle, remaining essentially constant over the first four. In the fifth cycle, however, the catalyst managed to convert 4-nitrophenol (4-NP) to 4-aminophenol (4-AP) completely in just 22 minutes. Significantly, following the fifth cycle, the pseudo-first-order rate constant ($k = 2.58 \times 10^{-3}\ s^{-1}$) stayed comparatively high, hence bolstering the catalyst's structural soundness, reusability, and long-term catalytic effectiveness.

7.6 Effect of pH

The impact of pH on dye degradation is primarily controlled by its effects on the catalyst's surface charge properties and the ionisation state of dye molecules, which collectively determine dye catalyst interactions and reaction efficiency. Changes in pH cause surface functional groups on the catalyst to either protonate or deprotonate, changing the surface charge density. Protonation makes the catalyst surface positively charged at pH values below the point of zero charge (pH_pzc), which enhances electrostatic attraction and adsorption of anionic dyes, while deprotonation produces a negatively charged surface at pH values above the pH_pzc, which preferentially adsorbs cationic dyes while repelling anionic species. Dye molecules' chemical structure, ionisation state, solubility, and molecular conformation are all simultaneously altered by pH, which has an impact on the molecules' reactivity. While electrostatic repulsion under unfavourable pH conditions restricts adsorption and access to active sites, decreasing degradation efficiency, favourable electrostatic interactions between oppositely charged dye molecules and catalyst surfaces enhance adsorption, promote efficient electron transfer, and accelerate degradation kinetics. Furthermore, especially in redox- and photocatalytic systems, pH can affect the stability of catalytic species, the production and accessibility of reactive intermediates, and the dominant degradation pathways. All of these factors point to pH as a crucial operational parameter that regulates dye catalyst interactions, surface charge modulation, and the general efficiency of catalytic dye degradation processes.[131] $NaBH_4$ is comparatively more stable under alkaline conditions. Thus, a stable co-catalyst accelerates the photo–catalytic reaction.

The pH of the solution determines the surface charge characteristics of the photocatalyst and the size of the aggregates it forms, making it a crucial parameter in the photocatalytic

processes occurring on particulate surfaces.[132] Therefore, pH affects dye properties as well as the reaction mechanisms, including hydroxyl radical attack, direct oxidation by the positive hole, and direct reduction by the electron in the conduction band that can lead to dye degradation. When a photocatalyst is present, it is assumed that the electron–hole pairs created on the semiconductor's surface by UV light irradiation are the likely cause of the photocatalytic reactions. The reactive dye is then either directly oxidised by the holes with the high oxidative potential or forms a hydroxyl radical through a reaction with the OH^-. The following reactions (8) and (9) might be used to express the whole interaction between the reactive dye and the photocatalyst.[126,132,133] Jara *et al.* (2024)[69] concluded that the breakdown of organic dyes occurs, while maintaining the other factors constant. The pH was adjusted between 2 and 12, and the ideal pH was determined (Fig. 7).

$$h_{VB}^{+} + OH^- \rightarrow {}^{\bullet}OH \quad (8)$$

$${}^{\bullet}OH + \text{dye} \rightarrow \text{degradation of the dye} \quad (9)$$

7.7 Initial concentration of dye

The quantity of dye in solution prior to any treatment or degradation process is known as the initial concentration of the dye, and it is commonly expressed in units such as mg L^{-1}, mol L^{-1} (M), or ppm. Various dye starting concentrations were examined in order to examine the impact of dye concentration on catalytic degradation efficiency.[69] The decolourisation rate constant (k) decreases as the dye concentration increases. There are two primary ways that the initial dye concentration might impact the rate of photodegradation. More active sites might have dye ions covering them at high dye concentrations. This might also result in less OH radicals being produced on the catalyst's surface. In the concentration range of 0.025–0.1 g L^{-1}, Ilinoiu *et al.* investigated the effects of different starting dye concentrations for reactive yellow 125 dye on the photocatalytic discolouration and degradation. They concluded that if the dye concentration is increased, the degradation efficiency would decrease, making the procedure less effective. When the initial concentration of methyl orange increases, the path length of the photons entering the solution reduces. The catalyst absorbed more photons as a result of the reversal that took place for the lower concentration (Fig. 8). In their investigation of the photocatalytic degradation of commercial dyes employing zinc oxide powder as a photocatalyst, the authors of ref. 134 discovered the same[135] outcome.[134–138]

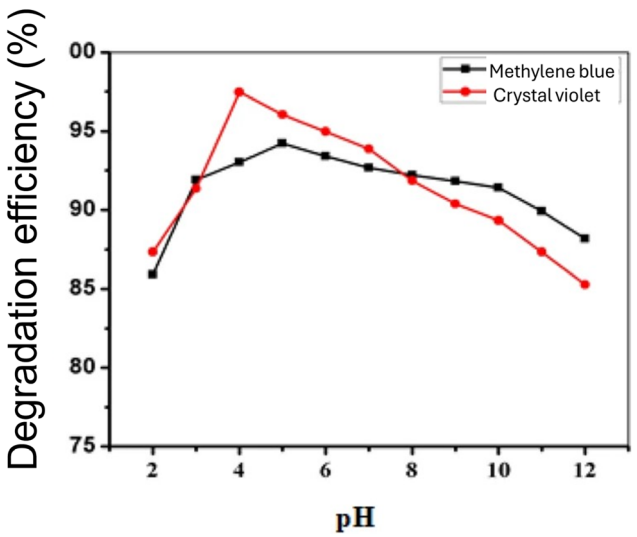

Fig. 7 In order to separate the impact of pH on degradation efficiency, the catalytic degradation of methylene blue (MB) and crystal violet (CV) was investigated under controlled conditions. In order to influence dye–catalyst interactions, pH was discovered to be a critical element impacting catalyst surface charge, dye ionisation, and redox potential. Insights into how acidic or alkaline environments control electron transport during dye reduction were gained by determining the ideal pH for optimal catalytic activity by altering pH while holding other parameters constant, adapted/reproduced from ref. 69 with permission from Springer Nature [*Scientific Reports*], copyright 2024.

8. Nanoclusters for dye degradation with $NaBH_4$ as a co-catalyst

A glutathione-capped silver nanocluster (GSH@Ag NCs) was synthesised using L-glutathione (GSH) and silver nitrate ($AgNO_3$). First, two solutions were made: one was a 20 mM aqueous solution of GSH, and the other was a 20 mM $AgNO_3$ solution in deionised water. Furthermore, 10 mL of 0.1 M NaOH was used to dissolve 42 mg of freshly made sodium borohydride ($NaBH_4$), resulting in a final concentration of 114 mM. 4.4 mL of deionised water was mixed with 0.375 mL of the GSH solution and 0.125 mL of the $AgNO_3$ solution for the synthesis. At room temperature, this mixture was constantly agitated to promote the development of Ag(I) GSH complexes. 50 μL of the freshly made $NaBH_4$ solution was added dropwise after the complex had formed. The solution became deep crimson in about five

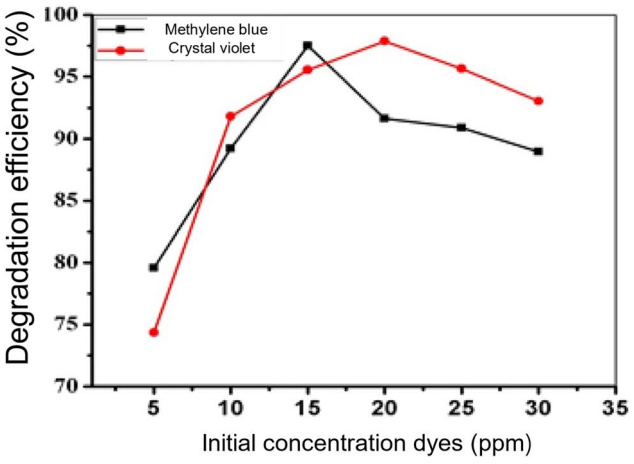

Fig. 8 Impact of starting dye concentration on methylene blue (MB) and crystal violet (CV) catalytic degradation, adapted/reproduced from ref. 69 with permission from Springer Nature [*Scientific Reports*], copyright 2024.

minutes, a sign that silver nanoclusters were forming. The deep red Ag nanoclusters were then allowed to break down again into colourless Ag(I) GSH complexes by leaving the reaction mixture undisturbed at ambient temperature for four hours. A further 50 μL of the $NaBH_4$ solution was then added after the mixture had been forcefully agitated once more. The solution progressively turned dark and light brown after 30 minutes of reaction. GSH@Ag NCs were successfully formed by the last stage, which was to incubate the mixture for eight hours at room temperature without stirring. After purification, the produced nanoclusters were kept for later use at 4 °C. The presence of nanoclusters was verified by UV-vis spectroscopy, which displayed a distinctive absorbance peak at 489 nm. The end result showed up as a brown solution with silver nanoclusters stabilised by GSH.[139]

$$\text{Dye degradation } \% = A_0 - A_t/A_0 \times 100\% = (C_0 = C/C_0) \times 100\% \quad (10)$$

Electron transport between the dye molecules and the artificial glutathione-capped silver nanoclusters (GSH@Ag NCs) is the main mechanism of degradation. In a recent study, we used water-soluble GSH@Ag NCs to report for the first time the photocatalytic degradation of xanthene dyes, specifically erythrosine B (Ery. B) and rhodamine B (Rh. B). Excellent dye degradation was demonstrated by the nanoclusters. At the Ag nanoclusters' surface, where the dye molecules and sodium borohydride ($NaBH_4$), a potent reducing agent, are adsorbed, the electron transfer process takes place. By reducing the activation energy needed for the reaction, the adsorption of $NaBH_4$ onto the Ag nanocluster surface speeds up the catalytic process. The dye molecules break down structurally in this state, producing CO_2 and H_2O as byproducts. The oxidation–reduction (redox) process starts the breakdown of the xanthene dyes when they acquire electrons. Both GSH@Ag NCs and $NaBH_4$ work in concert to promote photodegradation in this system. The process entails photoexcitation of the Ag nanoclusters under visible light irradiation, which facilitates electron transport to the dye molecules and increases their reduction and breakdown. For each dye, different mechanistic paths are suggested under visible light, one of which is a well-known photocatalytic pathway involving the creation of electron–hole pairs by light and the ensuing redox reactions.[139–147]

$$\text{Xanthene dyes} + h\nu + \text{xanthene dyes}$$

$$\text{GSH@Ag NCs} + h\nu \rightarrow (e^-) + h^+ \ (e_{CB}{}^- + h_{VB}{}^+)$$

$$(O_2)_{ads} + (e_{CB}{}^-) \rightarrow (O_2{}^{\bullet -})_{ads}$$

The photodegraded holes can be oxidized with water to produce OH*.

$$Ag + OH + h\nu^+ \rightarrow Ag + OH^*$$

$$Ag + H_2O + h_{VB}{}^+ \rightarrow Ag + OH^* + H^+$$

$$\text{Xanthene dyes} + h^+ \rightarrow \text{xanthene dyes or degradation products (oxidation reaction)}$$

9. Nanoparticles V/S nanoclusters for dye degradation

The unique physicochemical characteristics of nanoparticles and nanoclusters have a significant impact on how well they function in dye degradation processes. While catalytic activity in nanoparticles is primarily restricted to surface atoms, the ultrasmall size of nanoclusters offers an extraordinarily high surface-to-volume ratio, leading to a substantial fraction of surface-exposed atoms that operate as active catalytic sites. For nanoclusters, this inherent structural variation results in improved catalytic effectiveness and quicker dye degradation kinetics, especially in electron-transfer-mediated reduction processes. From an optical perspective, nanoclusters lack plasmonic behaviour and instead display molecule-like fluorescence because of discrete electronic energy levels, whereas nanoparticles, particularly noble metals like gold and silver,[80] display specific surface plasmon resonance, which improves photocatalytic dye degradation by enhancing light absorption and charge carrier generation. Nanoparticles are more frequently used materials in practical dye wastewater treatment, while nanoclusters are mainly investigated in high-efficiency and mechanistic dye degradation studies, despite their superior catalytic activity and effectiveness at lower catalyst loadings. However, the widespread application of nanoclusters is limited by issues related to colloidal stability, higher cost, and scalability. Nanoclusters are atomically precise particles. They are highly sensitive towards experimental conditions.[148] During the photocatalytic process, nanoclusters (photocatalyst) are often aggregated in the presence of the co-catalyst (H_2O_2, $NaBH_4$) and the pollutant (dyes). Consequently, the report of nanocluster-induced dye degradation is compared to nanoparticle-induced dye degradation. Moreover, nanoclusters often lose their identity with external energy sources, inevitable for dye degradation. We found only a few papers on dye degradation with nanoclusters, unlike nanoparticles. Nanoparticles have plentiful reports for dye degradation with $NaBH_4$.[91]

10. Effects of scavengers

Radical scavengers are used as diagnostic tools in dye degradation studies, particularly in photocatalytic and advanced oxidation processes, to determine which reactive species such as hydroxyl radicals (OH), superoxide radical anions ($O_2{}^-$), photo-generated holes (h^+), or electrons (e^-) are primarily in charge of degrading dye molecules. Researchers can see how much the degrading efficiency is lowered by adding a scavenger that specifically neutralises one type of reactive species; a significant decline suggests that the targeted species is important. For example, the inclusion of $^{\bullet}OH$ and $^{\bullet}O_2{}^-$ scavengers (such as 2-propanol or *p*-benzoquinone) significantly decreased dye removal (to 0.4–1.6%) in the visible-light

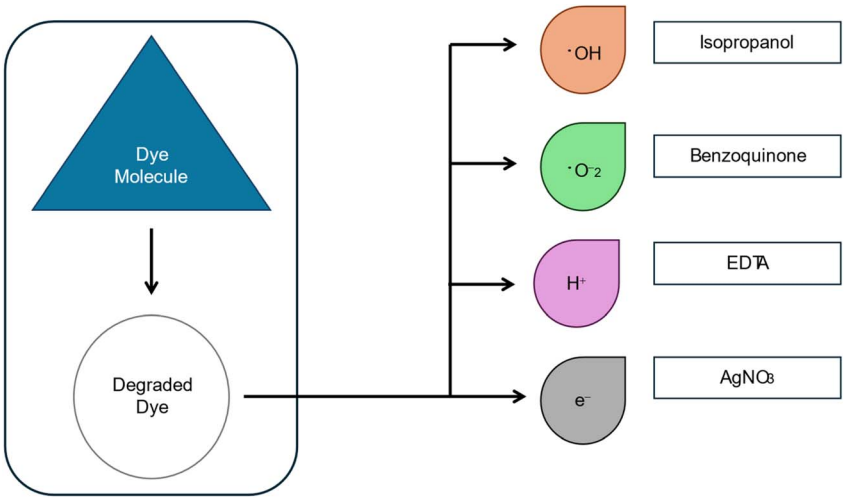

Fig. 9 Diagrammatic representation of the effects of scavengers in dye degradation.

photocatalytic degradation of rhodamine B using WO_3, indicating that these radicals are the primary contributors.[149] The breakdown of gentian violet using FeO_3/MgO nanocomposites is another recent example. The efficiency dramatically decreased when EDTA and methanol were employed as scavengers, demonstrating the participation of holes and hydroxyl radicals. Such tests allow for optimisation (selecting catalysts or settings that enhance synthesis of the effective radicals), assist clarification processes (which radical is dominant under what conditions), and prevent misunderstanding (because certain species may appear but have little real impact) (Fig. 9). Recent research has shown a warning: findings should be carefully interpreted since scavengers or interfering species might occasionally complicate them (for example, by producing secondary radicals or causing side reactions).[150,151]

11. $NaBH_4$ for nanoparticle synthesis V/S $NaBH_4$ for dye degradation

The size, morphology, dispersion, and catalytic performance of noble metal nanoparticles like Ag, Au, and Pd are significantly influenced by the concentration of $NaBH_4$, which is crucial in controlling the reduction kinetics of metal precursors and the nucleation-growth dynamics of these particles. Slow and kinetically regulated reduction at low concentrations of $NaBH_4$ results in restricted nucleation followed by prolonged growth, resulting in bigger, polydisperse, and often aggregated nanoparticles with lower electron-transfer efficiency and fewer accessible active sites. Higher $NaBH_4$ concentrations, on the other hand, accelerate electron and hydride transfer, causing burst nucleation and producing smaller, more evenly distributed nanoparticles with high surface-to-volume ratios. On the other hand, excessively high $NaBH_4$ levels can cause aggregation, borate surface passivation, or hydrogen-related defects that jeopardise long-term stability. Further modulating these effects is metal-specific behaviour: to create well-dispersed nanoparticles with low surface oxidation and high surface plasmon resonance (SPR), which facilitates effective electron shuttling during catalytic processes, Ag^+ is quickly reduced at moderate $NaBH_4$ concentrations. Because of Au's high work function and chemical inertness, which favour electron accumulation and prolonged catalytic activity, Au^{3+} reduction is particularly sensitive to $NaBH_4$ concentration, where ideal values are needed to avoid incomplete reduction and generate stable, monodisperse particles; higher concentrations of $NaBH_4$ can result in hydrogen absorption, lattice expansion, and defect formation; however, Pd compensates through superior surface redox activity and strong adsorption of organic substrates. Pd^{2+} reduction is relatively slower and is influenced by Pd's strong hydrogen affinity. Overall, the electronic structure, Fermi level alignment, surface plasmon effects (for Ag and Au), hydrogen affinity and redox behaviour (for Pd), and density of active surface sites of Ag, Au, and Pd nanoparticles determine their catalytic efficiency. These factors are all closely regulated by the concentration of $NaBH_4$ used during synthesis and catalytic operation.[69,98,145,152,153]

Strong reducing agents like sodium borohydride ($NaBH_4$) are frequently used in the manufacturing of metal nanoparticles (MNPs) such as Au, Ag, Pt, Pd, and Fe. $NaBH_4$ breaks down in aqueous solution to produce hydrogen gas and hydridic species (H^-) (Fig. 10), which act as the main reducing agents in the process, which involves the reduction of metal salt precursors (such as $AgNO_3$, $HAuCl_4$, and $FeCl_3$). Through the reduction process, metal ions (M^{n+}) are changed into zero-valent metal atoms (M^0). These atoms then nucleate through atomic collision and aggregation, grow, and form nanoparticles. In order to control the size and shape of the nanoparticles and avoid uncontrolled agglomeration, stabilising or capping agents like citrate, polyvinylpyrrolidone (PVP), or biomolecules derived from plants are usually added during synthesis.[154] Sodium borohydride ($NaBH_4$) is a potent reductant; its direct reduction of big, stable dye molecules is kinetically hampered even if it is thermodynamically advantageous. Ag, Au, Fe, and Pd metal nanoparticles (NPs) are used as catalysts to promote electron

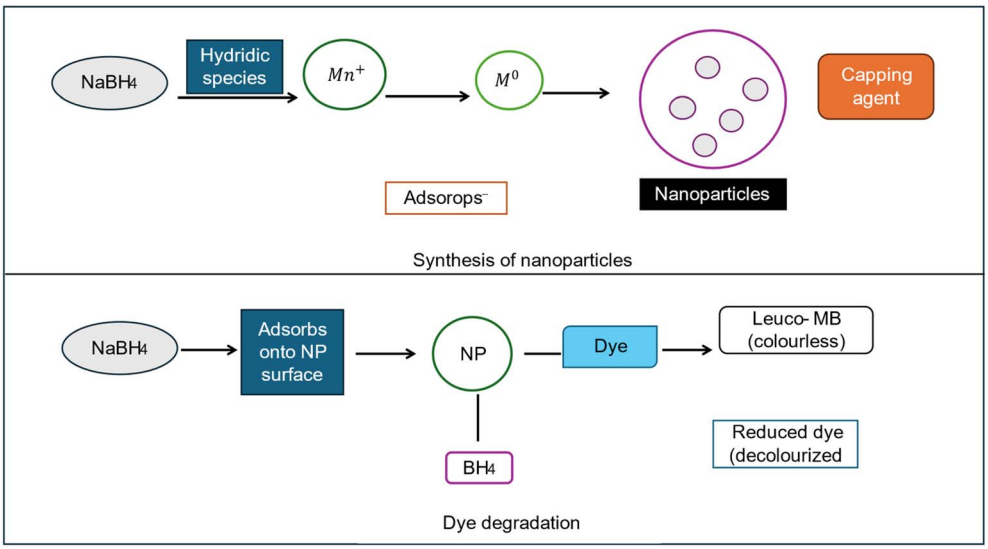

Fig. 10 Role of $NaBH_4$ in nanoparticle synthesis and dye degradation.

transport in order to overcome this restriction. This mechanism involves dye molecules adsorbing onto the same catalytic sites at the same time as $NaBH_4$ adsorbs onto the NP surface and produces hydride ions (H^-). The reduction reaction is accelerated by the nanoparticles' role as electron mediators, which involves moving electrons from BH_4^- to the dye. As demonstrated by the conversion of methylene blue (MB) into its colourless leuco-methylene blue (leuco-MB) by the transfer of two electrons and a proton in the presence of $NaBH_4$ and NPs, this causes the dye to change into its reduced (Fig. 10), decolorised form.[155]

12. Conclusions

The mechanistic elements of $NaBH_4$-assisted catalytic degradation are still poorly understood despite a great deal of research, especially when it comes to hydride transfer routes, catalyst-mediated electron relay mechanisms, and the nature of transitory reaction intermediates. Additionally, during numerous $NaBH_4$ reaction cycles, many metal and metal-oxide catalysts experience surface oxidation, particle aggregation, and borate-induced surface passivation, which severely reduces their catalytic stability and reusability. Comprehensive understanding of reaction dynamics is hindered by the majority of current research, which mostly uses pseudo-first-order kinetic models with little investigation of specific kinetic and thermodynamic parameters. Concerns about the long-term environmental sustainability of degradation intermediates and borate byproducts produced *via* $NaBH_4$-assisted processes are also raised by the lack of research on their destination, toxicity, and environmental effects.

Advanced spectroscopic methods like *in situ* FT-IR, electron paramagnetic resonance (EPR), time-resolved UV-visible spectroscopy, and mass spectrometry should be methodically used to clarify the formation of chemical intermediates and pinpoint rate-determining steps in $NaBH_4$-assisted degradation processes. Additionally, to improve resistance against surface oxidation and borate adsorption and to increase catalytic stability and reusability, surface-engineered catalysts such as core–shell designs, doped systems, and hybrid nanostructures must be developed. Comprehensive kinetic modelling, activation energy determination, and reaction thermodynamic analysis should be carried out in order to enhance process predictability and mechanistic knowledge. To guarantee the long-term environmental safety and sustainability of $NaBH_4$-assisted treatment methods, a thorough evaluation of the ecotoxicity, biodegradability, and environmental destiny of degradation products and residual borate species is also essential.

Conflicts of interest

The authors declare that they have no known competing financial interests or personal relationships that could have appeared to influence the work reported in this paper.

Data availability

No primary research results, software or code has been included.

References

1 P. Sharma, M. Ganguly and M. Sahu, Role of transition metals in coinage metal nanoclusters for the remediation of toxic dyes in aqueous systems, *RSC Adv.*, 2024, **14**, 11411–11428.
2 C. K. Wong, P. P. K. Wong and L. M. Chu, Heavy metal concentrations in marine fishes collected from fish culture sites in Hong Kong, *Arch. Environ. Contam. Toxicol.*, 2001, **40**, 60–69.

3 W. Ashraf, Accumulation of heavy metals in kidney and heart tissues of Epinephelus Micrdon fish from the Arabian Gulf, *Environ. Monit. Assess.*, 2005, **101**, 311–316.
4 F. A. A. Muataz Ali Atieh, O. Yahya Bakather, B. S. Tawabini, A. A. Bukhari, M. Khaled, M. Alharthi and M. Fettouhi, Removal of Chromium (III) from Water by Using Modified and Nonmodified Carbon Nanotubes, *J. Nanomater.*, 2010, **2010**(1), 232378.
5 I. O. Ángela Anglada and A. Urtiaga, Contributions of electrochemical oxidation to waste-water treatment: fundamentals and review of applications, *J. Chem. Technol. Biotechnol.*, 2009, **84**, 1747–1755.
6 Y. M. Awad and N. S. Abuzaid, Electrochemical Treatment of Phenolic Wastewater: Efficiency, Design Considerations and Economic Evaluation, *J. Environ. Sci. Health, Part A: Toxic/Hazard. Subst. Environ. Eng.*, 1997, **32**, 1393–1414.
7 S. Ayoob and A. K. Gupta, Fluoride in drinking water: A review on the status and stress effects, *Crit. Rev. Environ. Sci. Technol.*, 2006, **36**, 433–487.
8 S. Vasudevan and M. A. Oturan, Electrochemistry: As cause and cure in water pollution-an overview, *Environ. Chem. Lett.*, 2014, **12**, 97–108.
9 T. S. Natarajan, M. Thomas, K. Natarajan, H. C. Bajaj and R. J. Tayade, Study on UV-LED/TiO2 process for degradation of Rhodamine B dye, *Chem. Eng. J.*, 2011, **169**, 126–134.
10 B. Gupta, M. Rani, R. Salunke and R. Kumar, In vitro and in vivo studies on degradation of quinalphos in rats, *J. Hazard. Mater.*, 2012, **213–214**, 285–291.
11 A. B. Prevot, C. Baiocchi, M. C. Brussino, E. Pramauro, P. Savarino, V. Augugliaro, G. Marci and L. Palmisano, Photocatalytic degradation of Acid Blue 80 in aqueous solutions containing TiO2 suspensions, *Environ. Sci. Technol.*, 2001, **35**, 971–976.
12 C. Sahoo, A. K. Gupta and A. Pal, Photocatalytic degradation of Methyl Red dye in aqueous solutions under UV irradiation using Ag+ doped TiO2, *Desalination*, 2005, **181**, 91–100.
13 I. Bazin, A. Ibn Hadj Hassine, Y. Haj Hamouda, W. Mnif, A. Bartegi, M. Lopez-Ferber, M. De Waard and C. Gonzalez, Estrogenic and anti-estrogenic activity of 23 commercial textile dyes, *Ecotoxicol. Environ. Saf.*, 2012, **85**, 131–136.
14 W. Zhang and C. W. Wu, Dyeing of multiple types of fabrics with a single reactive azo disperse dye, *Chem. Pap.*, 2014, **68**, 330–335.
15 Z. Carmen and S. Daniela, *Characteristics , Polluting Effects and Separation/Elimination Procedures from Industrial Effluents – A Critical Overview*, Text Org Dye, 2010, pp. 55–86.
16 D. Mohan, K. P. Singh, G. Singh and K. Kumar, *Removal of Dyes from Wastewater Using Flyash, a Low-Cost.Pdf*, 2002, pp. 3688–3695.
17 W. L. Kostedt IV, A. A. Ismail and D. W. Mazyc, Impact of heat treatment and composition of ZnO-TiO2 nanoparticles for photocatalytic oxidation of an azo dye, *Ind. Eng. Chem. Res.*, 2008, **47**, 1483–1487.
18 A. Safavi and S. Momeni, Highly efficient degradation of azo dyes by palladium/hydroxyapatite/Fe 3O 4 nanocatalyst, *J. Hazard. Mater.*, 2012, **201–202**, 125–131.
19 B. S. Padhi, Pollution due to synthetic dyes toxicity & carcinogenicity studies and remediation, *Int. J. Environ. Sci.*, 2012, **3**, 940–955.
20 U. Shanker, M. Rani and V. Jassal, Degradation of hazardous organic dyes in water by nanomaterials, *Environ. Chem. Lett.*, 2017, **15**, 623–642.
21 S. Bhattacharya, I. Saha, A. Mukhopadhyay, D. Chattopadhyay and U. Chand, Role of nanotechnology in water treatment and purification: Potential applications and implications, *Int. J. Chem. Sci. Technol.*, 2013, **3**(3), 59.
22 D. Nunes, A. Pimentel, R. Branquinho, E. Fortunato and R. Martins, Metal Oxide-Based Photocatalytic Paper: A Green Alternative for Environmental Remediation, *Catalysts*, 2021, **11**, 504.
23 W. MacSwain, D.-K. Ma, Z.-J. Li, H. Lin, Y.-L. Bai, X. Hu and W. Zheng, Metal-based co-catalysts in semiconductor CdS hybrid nanostructures for enhanced photocatalysis: material design, mechanisms, and emerging trends, *Coord. Chem. Rev.*, 2026, **549**, 217247.
24 M. Sahu, M. Ganguly and P. Sharma, Role of silver nanoparticles and silver nanoclusters for the detection and removal of Hg(ii), *RSC Adv.*, 2024, **14**, 22374–22392.
25 C. S. Bhatt, B. Nagaraj and A. K. Suresh, Nanoparticles-shape influenced high-efficient degradation of dyes: Comparative evaluation of nano-cubes vs. nano-rods vs. nano-spheres, *J. Mol. Liq.*, 2017, **242**, 958–965.
26 S. Veziroglu, A. L. Obermann, M. Ullrich, M. Hussain, M. Kamp, L. Kienle, T. Leißner, H. G. Rubahn, O. Polonskyi, T. Strunskus, J. Fiutowski, M. Es-Souni, J. Adam, F. Faupel and O. C. Aktas, Photodeposition of Au Nanoclusters for Enhanced Photocatalytic Dye Degradation over TiO2 Thin Film, *ACS Appl. Mater. Interfaces*, 2020, **12**, 14983–14992.
27 A. Molla and J. H. Youk, Chemical clock reactions with organic dyes: Perspective, progress, and applications, *Dyes Pigm.*, 2022, **202**, 110237.
28 H. Abazied Shindy, Basics in colors, dyes and pigments chemistry: A review, *Chem. Int.*, 2016, **2**, 29–36.
29 H. A. Shindy, *Problems and Solutions in Colors, Dyes and Pigments Chemistry: a Review*, 2017, vol. 3, pp. 97–105.
30 D. M. Lewis, Developments in the chemistry of reactive dyes and their application processes, *Color. Technol.*, 2014, **130**, 382–412.
31 I. Arslan-Alaton, A review of the effects of dye-assisting chemicals on advanced oxidation of reactive dyes in wastewater, *Color. Technol.*, 2003, **119**, 345–353.
32 A. Akinyemi, O. Agboola, E. Alagbe and E. Igbokwe, The role of catalyst in the adsorption of dye: Homogeneous catalyst, heterogeneous catalyst, and advanced catalytic activated carbon, critical review, *Desalin. Water Treat.*, 2024, **320**, 100780.
33 J. Prakash, Mechanistic Insights into Graphene Oxide Driven Photocatalysis as Co-Catalyst and Sole Catalyst in

Degradation of Organic Dye Pollutants, *Photochem*, 2022, **2**, 651–671.

34 G. A. P. Murat Oz and D. E. Lorke, Mohammed Hasan, Cellular and MolecularActions of Methylene Blue in the Nervous System, *Harv. Bus. Rev.*, 2008, **86**, 84–92.

35 T. Cwalinski, W. Polom, L. Marano, G. Roviello, A. D'angelo, N. Cwalina, M. Matuszewski, F. Roviello, J. Jaskiewicz and K. Polom, Methylene blue—current knowledge, fluorescent properties, and its future use, *J. Clin. Med.*, 2020, **9**(11), 3538.

36 J. C. Bollinger, E. C. Lima, L. Mouni, S. Salvestrini and H. N. Tran, Molecular properties of methylene blue, a common probe in sorption and degradation studies: a review, *Environ. Chem. Lett.*, 2025, **23**, 1403–1424.

37 I. Khan, K. Saeed, I. Zekker, B. Zhang, A. H. Hendi, A. Ahmad, S. Ahmad, N. Zada, H. Ahmad, L. A. Shah, T. Shah and I. Khan, Review on Methylene Blue: Its Properties, Uses, Toxicity and Photodegradation, *Water*, 2022, **14**(2), 242.

38 A. A. Al-Muntaser, S. A. Al-Ghamdi, E. Alzahrani, A. Rajeh, G. M. Asnag, A. M. Al-Harthi, R. Alwafi, A. Saeed, S. Aldwais and A. Y. Yassin, Investigation of structural and optical characteristics of PVA/crystal violet dye composites for flexible smart optoelectronic applications, *J. Polym. Res.*, 2024, **31**, 1–11.

39 S. Mani and R. N. Bharagava, Exposure to crystal violet, its toxic, genotoxic and carcinogenic effects on environment and its degradation and detoxification for environmental safety, *Rev. Environ. Contam. Toxicol.*, 2016, **237**, 71–104.

40 P. Rajesh, A. Silambarasan and P. Ramasamy, Effect of crystal violet dye on the optical, dielectric, thermal and mechanical properties of ⟨0 0 1⟩ directed KDP single crystal, *Mater. Res. Bull.*, 2014, **49**, 640–644.

41 S. Goel, N. Sinha, H. Yadav, A. Hussain and B. Kumar, Effect of crystal violet dye on the structural, optical, mechanical and piezoelectric properties of ADP single crystal, *Mater. Res. Bull.*, 2016, **83**, 77–87.

42 R. Ragu, P. S. L. Mageshwari, M. Akilan and S. J. Das, Enhanced optical, mechanical, photoacoustic and third-order nonlinear property of pure and crystal violet (CV) dye incorporated anthracene crystal: an efficacious material for nonlinear optical applications, *Appl. Phys. B:Lasers Opt.*, 2020, **126**, 1–10.

43 L. Sellaoui, G. L. Dotto, E. C. Peres, Y. Benguerba, É. C. Lima, A. Ben Lamine and A. Erto, New insights into the adsorption of crystal violet dye on functionalized multi-walled carbon nanotubes: Experiments, statistical physics and COSMO–RS models application, *J. Mol. Liq.*, 2017, **248**, 890–897.

44 T. L. Yusuf, B. O. Orimolade, D. Masekela, B. Mamba and N. Mabuba, The application of photoelectrocatalysis in the degradation of rhodamine B in aqueous solutions: a review, *RSC Adv.*, 2022, **12**, 26176–26191.

45 Z. M. Saig, Various Adsorbents for Removal of Rhodamine B Dye: A Review, *Indones. J. Chem.*, 2021, **21**, 1039–1056.

46 M. Danish, T. Ahmad, R. Hashim, N. Said, M. N. Akhtar, J. Mohamad-Saleh and O. Sulaiman, *Comparison of Surface Properties of Wood Biomass Activated Carbons and Their Application against Rhodamine B and Methylene Blue Dye*, Elsevier B.V., 2018, vol. 11.

47 N. Bar and P. Chowdhury, A Brief Review on Advances in Rhodamine B Based Chromic Materials and Their Prospects, *ACS Appl. Electron. Mater.*, 2022, **4**, 3749–3771.

48 M. Islam, M. Hossain, S. Mahbub, M. A. Hoque, D. Kumar, S. M. Wabaidur, M. A. Habila, M. M. AL-Anazy and M. Kabir, Influences of alcohol and diol on the aggregation behaviour, modes of interaction and the thermodynamic properties of the mixture of bromocresol green dye and sodium dodecyl sulphate at numerous temperatures, *Mol. Phys.*, 2021, **119**(12), e1925364.

49 H. Wen, C. Ou, H. Tang, S. Sang, Y. Du and J. Chen, Development, Characterization and Application of a Three-Layer Intelligent pH-Sensing Indicator Based on Bromocresol Green (BCG) for Monitoring Fish Freshness, *J. Ocean Univ. China*, 2023, **22**, 565–575.

50 C. Elijah Onu, C. Oluchukwu Asadu, P. Enyinnaya Ohale, C. Nkeiruka Nweke, I. Chukwudi Nwokedi, N. Nwabanwanne Musei and C. Peace Onu, Adsorptive removal of bromocresol green dye using activated corn cob, *J. Eng. Appl. Sci.*, 2022, **21**, 824–841.

51 O. Chijioke Elijah, O. Nonso Collins, O. Callistus Obumneme and N.-B. Jessica, Application of Modified Agricultural Waste in the Adsorption of Bromocresol Green Dye, *Asian J. Chem. Sci.*, 2020, **7**, 15–24.

52 A. M. El-Didamony, S. M. Hafeez and A. A. Saad, Application of bromocresol green and bromothymol blue for the extractive spectrophotometric determination of anti-hypertensive drugs, *J. Appl. Pharm. Sci.*, 2015, **5**, 122–129.

53 P. Martelli, R. Caputo, A. Remhof, P. Mauron, A. Borgschulte and A. Züttel, Stability and decomposition of NaBH4, *J. Phys. Chem. C*, 2010, **114**, 7173–7177.

54 P. Fischer and A. Züttel, Order-Disorder Phase Transition in NaBD4, *Mater. Sci. Forum*, 2004, **443–444**, 287–290.

55 H. L. Johnston and N. C. Hallett, Low Temperature Heat Capacities of Inorganic Solids. XIV. Heat Capacity of Sodium Borohydride from 15-300°K, *J. Am. Chem. Soc.*, 1953, **75**, 1467–1468.

56 W. H. Stockmayer and C. C. Stephenson, The nature of the gradual transition in sodium borohydride, *J. Chem. Phys.*, 1953, **21**, 1311–1312.

57 J. Abrahams and S. C. Kalnajs, The Lattice Constants of the Alkali Borohydrides and the Low-Temperature Phase of Sodium Borohydride, *J. Chem. Phys.*, 1954, **22**, 434–436.

58 R. L. Davis and C. H. L. Kennard, Structure of sodium tetradeuteroborate, NaBD4, *J. Solid State Chem.*, 1985, **59**, 393–396.

59 D. G. Allis and B. S. Hudson, Inelastic neutron scattering spectra of NaBH4 and KBH 4: Reproduction of anion mode shifts via periodic DFT, *Chem. Phys. Lett.*, 2004, **385**, 166–172.

60 Y. Filinchuk and H. Hagemann, Structure and properties of NaBH4·2H2O and NaBH4, *Eur. J. Inorg. Chem.*, 2008, **2008**, 3127–3133.

61 T. Salmi and V. Russo, Reaction engineering approach to the synthesis of sodium borohydride, *Chem. Eng. Sci.*, 2019, **199**, 79–87.
62 Z. Gao, B. Yao, L. Ji and T. Xu, Effect of Reducing Agent NaBH4 on Photocatalytic Properties of Bi/BiOBr/Bi2WO6 Composites, *ChemistrySelect*, 2019, **4**, 10065–10071.
63 U. T. Khatoon, A. Velidandi and G. V. S. Nageswara Rao, Sodium borohydride mediated synthesis of nano-sized silver particles: Their characterization, anti-microbial and cytotoxicity studies, *Mater. Chem. Phys.*, 2023, **294**, 126997.
64 N. Ahmed, D. Vione, L. Rivoira, L. Carena, M. Castiglioni and M. C. Bruzzoniti, A review on the degradation of pollutants by fenton-like systems based on zero-valent iron and persulfate: Effects of reduction potentials, ph, and anions occurring in waste waters, *Molecules*, 2021, **26**(15), 4584.
65 N. N. Roslan, H. L. H. Lau, N. A. A. Suhaimi, N. N. M. Shahri, S. B. Verinda, M. Nur, J. W. Lim and A. Usman, Recent Advances in Advanced Oxidation Processes for Degrading Pharmaceuticals in Wastewater—A Review, *Catalysts*, 2024, **14**, 1–25.
66 P. Sharma, S. Kar, M. Sahu and M. Ganguly, Copper-based nanoparticles for the removal of the crystal violet dye via degradation and adsorption: a comparative account, *RSC Adv.*, 2025, **15**, 27995–28020.
67 N. K. Akbaş and B. Kutlu, Effect of hydroxyl (·OH) radicals on the progression of NaBH4 hydrolysis reaction on fcc-Co surfaces: A DFT study, *Phys. B*, 2022, **647**, 414385.
68 L. Yu and M. A. Matthews, Hydrolysis of sodium borohydride in concentrated aqueous solution, *Int. J. Hydrogen Energy*, 2011, **36**, 7416–7422.
69 Y. S. Jara, T. T. Mekiso and A. P. Washe, Highly efficient catalytic degradation of organic dyes using iron nanoparticles synthesized with Vernonia Amygdalina leaf extract, *Sci. Rep.*, 2024, **14**, 1–18.
70 F. A. Carey and R. J. Sundberg, Planning and Execution of Multistep Syntheses, *Adv. Org. Chem.*, 2006, 821–922.
71 F. A. Carey and R. J. Sundberg, Nucleophilic Substitution, *Adv. Org. Chem.*, 2006, 263–350.
72 E. Ramos, S. F. Calatrava and L. Jiménez, Bleaching with hydrogen peroxide. A review, *Afinidad*, 2008, **65**, 366–373.
73 S. C. Amendola, S. L. Sharp-Goldman, M. S. Janjua, N. C. Spencer, M. T. Kelly, P. J. Petillo and M. Binder, A Safe, portable, hydrogen gas generator using aqueous borohydride solution and Ru catalyst, *Int. J. Hydrogen Energy*, 2000, **25**, 969–975.
74 M. L. Christian and K.-F. Aguey-Zinsou, Core–Shell Strategy Leading to High Reversible Hydrogen Storage Capacity for NaBH4, *ACS Nano*, 2012, **6**, 7739–7751.
75 S. Wacławek, H. V. Lutze, K. Grübel, V. V. T. Padil, M. Černík and D. D. Dionysiou, Chemistry of persulfates in water and wastewater treatment: A review, *Chem. Eng. J.*, 2017, **330**, 44–62.
76 S. W. Chaikin and W. G. Brown, Reduction of Aldehydes, Ketones and Acid Chlorides by Sodium Borohydride, *J. Am. Chem. Soc.*, 1949, **71**, 122–125.
77 S. Shin, Y. Kim, J.-H. Jin and J. Jung, Heat-Induced Dry Hydrolysis of Sodium Borohydride/Oxalic Acid Dihydrate Composite for Hydrogen Production, *ACS Omega*, 2021, **7**, 979–986.
78 P. Pędziwiatr, Decomposition of Hydrogen Peroxide - Kinetics and Review of Chosen Catalysts, *Acta Innov.*, 2018, **26**, 45–52.
79 Z. C. Lu and L. T. Zhang, Recent advances in sodium borohydride for hydrogen storage, *E3S Web Conf.*, 2023, **385**, 04025.
80 D. M. F. Santos and C. A. C. Sequeira, Sodium borohydride as a fuel for the future, *Renewable Sustainable Energy Rev.*, 2011, **15**, 3980–4001.
81 H. Li, Y. Li, L. Sun, S. Xun, W. Jiang, M. Zhang, W. Zhu and H. Li, H2O2 decomposition mechanism and its oxidative desulfurization activity on hexagonal boron nitride monolayer: A density functional theory study, *J. Mol. Graphics Modell.*, 2018, **84**, 166–173.
82 Crystal and molecular structure of hydrogen peroxide: a neutron-diffraction study, https://pubchem.ncbi.nlm.nih.gov/compound/Hydrogen-Peroxide.
83 Y. Li, G. Liu, J. He and H. Zhong, Activation of Persulfate for Groundwater Remediation: From Bench Studies to Application, *Appl. Sci.*, 2023, **13**(3), 1304.
84 National Center for Biotechnology Information, PubChem Compound Summary for CID 24412, Potassium Persulfate, 2025, https://pubchem.ncbi.nlm.nih.gov/compound/Potassium-Persulfate.
85 C. R. Cloutier, A. Alfantazi and E. Gyenge, Physicochemical properties of alkaline aqueous sodium metaborate solutions, *J. Fuel Cell Sci. Technol.*, 2007, **4**, 88–98.
86 V. G. Minkina, S. I. Shabunya, V. I. Kalinin, V. V. Martynenko and A. L. Smirnova, Stability of alkaline aqueous solutions of sodium borohydride, *Int. J. Hydrogen Energy*, 2012, **37**, 3313–3318.
87 Y. Kojima, K. I. Suzuki, K. Fukumoto, Y. Kawai, M. Kimbara, H. Nakanishi and S. Matsumoto, Development of 10 kW-scale hydrogen generator using chemical hydride, *J. Power Sources*, 2004, **125**, 22–26.
88 V. G. Minkina, S. I. Shabunya, V. I. Kalinin, V. V. Martynenko and A. L. Smirnova, Stability of alkaline aqueous solutions of sodium borohydride, *Int. J. Hydrogen Energy*, 2012, **37**, 3313–3318.
89 Y. Shang and R. Chen, *Hydrogen Storage via the Hydrolysis of NaBH 4 Basic Solution: Optimization of NaBH 4 Concentration*, 2006, pp. 2142–2148.
90 A. J. Hung, S. F. Tsai, Y. Y. Hsu, J. R. Ku, Y. H. Chen and C. C. Yu, Kinetics of sodium borohydride hydrolysis reaction for hydrogen generation, *Int. J. Hydrogen Energy*, 2008, **33**, 6205–6215.
91 M. T. Kelly and J. V. Ortega, *Review of Chemical Processes for the Synthesis of Sodium Borohydride*, Millennium Cell Inc, 2004, pp. 1–24.
92 S. X. Chin, J. Vincent, N. F. Razak, N. Daud, S. Chowdhury, C. Wongchoosuk and C. H. Chia, Advancements and challenges in sodium borohydride hydrogen storage: A

comprehensive review of hydrolysis, regeneration, and recycling technologies, *J. Renewable Sustainable Energy*, 2025, **17**, 012702.

93 M. Dragan, Hydrogen Storage in Complex Metal Hydrides NaBH4: Hydrolysis Reaction and Experimental Strategies, *Catalysts*, 2022, **12**(4), 356.

94 V. I. Simagina, A. M. Ozerova, O. V. Komova and O. V. Netskina, Recent advances in applications of Co-B catalysts in NABH4-based portable hydrogen generators, *Catalysts*, 2021, **11**, 1–31.

95 C. Kaya, Sodium Borohydride (NaBH4) as a Maritime Transportation Fuel, *Hydrog*, 2024, **5**, 540–558.

96 U. B. Demirci and P. Miele, Sodium borohydride versus ammonia borane, in hydrogen storage and direct fuel cell applications, *Energy Environ. Sci.*, 2009, **2**, 627–637.

97 N. Pradhan, A. Pal and T. Pal, Silver nanoparticle catalyzed reduction of aromatic nitro compounds, *Colloids Surf., A*, 2002, **196**, 247–257.

98 S. N. Tan, M. L. Yuen and R. A. Ramli, Green Analytical Chemistry Photocatalysis of dyes : Operational parameters , mechanisms , and degradation pathway, *Green Anal. Chem.*, 2025, **12**, 100230.

99 M. M. Younus, M. A. Sayed, M. El Saied, A. O. Abo and E. Naga, Catalytic reduction of toxic dyes over nickel oxide nanoparticles supported on CMK - 3 catalyst, *Sci. Rep.*, 2024, 1–12.

100 W. Chen, Y. Chen, X. Zhu, M. Xu, Z. Han, L. Wang and L. Weng, NaBH4-Mediated Co-Reduction Synthesis of Glutathione Stabilized Gold/Silver Nanoclusters for Detection of Magnesium Ions, *Chemosensors*, 2023, **11**(8), 435.

101 G. Roland, D. Schäfer, T. Holtum, S. Küpper, A. Hoffmann and S. Schlücker, On the Overlooked Critical Role of the pH Value on the Kinetics of the 4-Nitrophenol NaBH4-Reduction Catalyzed by Noble-Metal Nanoparticles (Pt, Pd, and Au), *J. Phys. Chem. C*, 2020, **124**, 2939–2944.

102 Y. Li, H. Lu, Y. Wang and X. Li, Deposition of Au nanoparticles on PDA-functionalized PVA beads as a recyclable catalyst for degradation of organic pollutants with NaBH4 in aqueous solution, *J. Alloys Compd.*, 2019, **793**, 115–126.

103 A. A. Fairuzi, N. N. Bonnia, R. M. Akhir, M. A. Abrani and H. M. Akil, Degradation of methylene blue using silver nanoparticles synthesized from imperata cylindrica aqueous extract, *IOP Conf. Ser. Earth Environ. Sci.*, 2018, **105**, 012018.

104 S. A. Ogundare, T. O. Adesetan, G. Muungani, V. Moodley, J. F. Amaku, O. C. Atewolara-Odule, S. T. Yussuf, N. O. Sanyaolu, A. A. Ibikunle, M. S. Balogun and W. Ewald van Zyl, Catalytic degradation of methylene blue dye and antibacterial activity of biosynthesized silver nanoparticles using Peltophorum pterocarpum (DC.) leaves, *Environ. Sci.:Adv.*, 2022, **2**, 247–256.

105 J. Fabrega, S. N. Luoma, C. R. Tyler, T. S. Galloway and J. R. Lead, Silver nanoparticles: Behaviour and effects in the aquatic environment, *Environ. Int.*, 2011, **37**, 517–531.

106 T. Phenrat, N. Saleh, K. Sirk, R. D. Tilton and G. V. Lowry, Aggregation and Sedimentation of Aqueous Nanoscale Zerovalent Iron Dispersions, *Environ. Sci. Technol.*, 2006, **41**, 284–290.

107 K. Esumi, T. Hosoya, A. Suzuki and K. Torigoe, Spontaneous Formation of Gold Nanoparticles in Aqueous Solution of Sugar-Persubstituted Poly(amidoamine)dendrimers, *Langmuir*, 2000, **16**, 2978–2980.

108 W. Wang, Z. hui Jin, T. long Li, H. Zhang and S. Gao, Preparation of spherical iron nanoclusters in ethanol-water solution for nitrate removal, *Chemosphere*, 2006, **65**, 1396–1404.

109 N. Baig, I. Kammakakam, W. Falath and I. Kammakakam, Nanomaterials: A review of synthesis methods, properties, recent progress, and challenges, *Mater. Adv.*, 2021, **2**, 1821–1871.

110 P. Khanna, A. Kaur and D. Goyal, Algae-based metallic nanoparticles: Synthesis, characterization and applications, *J. Microbiol. Methods*, 2019, **163**, 105656.

111 R. S. Yehia and A. M. Ali, Biosynthesis and characterization of iron nanoparticles produced by Thymus vulgaris L. And their antimicrobial activity, *Acta Bot. Croat.*, 2020, **79**, 114–120.

112 S. K. Das, M. M. R. Khan, A. K. Guha, A. R. Das and A. B. Mandal, Silver-nano biohybride material: Synthesis, characterization and application in water purification, *Bioresour. Technol.*, 2012, **124**, 495–499.

113 S. Kanchana and R. Vijayalakshmi, Photocatalytic degradation of organic dyes by peg and pvp cappcu, ni and ag nanoparticles in the presence of nabh4 in aqueous medium, *J. Water Environ. Nanotechnol.*, 2020, **5**, 294–306.

114 D. Ayodhya and G. Veerabhadram, One-pot green synthesis, characterization, photocatalytic, sensing and antimicrobial studies of Calotropis gigantea leaf extract capped CdS NPs, *Mater. Sci. Eng., B*, 2017, **225**, 33–44.

115 Z. Yu, P. Zhu, L. Chen, G. Li, F. Zhou, D. D. Lu, R. Sun, F. Zhou and C. Wong, Hierarchical architectures of monodisperse porous Cu microspheres: synthesis, growth mechanism, high-efficiency and recyclable catalytic performance, *J. Mater. Chem. A*, 2014, **2**, 11966–11973.

116 L. Xiang-Zi, K.-L. Wu, Y. Ye and X.-W. Wei, Controllable synthesis of Ni nanotube arrays and their structure-dependent catalytic activity toward dye degradation, *CrystEngComm*, 2014, **16**, 4406–4413.

117 M. Meena Kumari, J. Jacob and D. Philip, Green synthesis and applications of Au-Ag bimetallic nanoparticles, *Spectrochim. Acta, Part A*, 2015, **137**, 185–192.

118 S. Aroob, S. A. C. Carabineiro, M. B. Taj, I. Bibi, A. Raheel, T. Javed, R. Yahya, W. Alelwani, F. Verpoort, K. Kamwilaisak, S. Al-Farraj and M. Sillanpää, Green Synthesis and Photocatalytic Dye Degradation Activity of CuO Nanoparticles, *Catalysts*, 2023, **13**, 1–18.

119 L. Zhang, S. Liu, Y. Wang, H. Zhang and F. Liang, Controllable Synthesis and Catalytic Performance of Gold

Nanoparticles with Cucurbit[n]urils (n = 5–8), *Nanomaterials*, 2018, **8**, 1015.

120 M. Ganguly, S. Dib and P. A. Ariya, Purely Inorganic Highly Efficient Ice Nucleating Particle, *ACS Omega*, 2018, **3**, 3384–3395.

121 H. Zheng, J. Huang, T. Zhou, Y. Jiang, Y. Jiang, M. Gao and Y. Liu, Recyclable Magnetic Cu/CuFe2O4 Nanocomposites for the Rapid Degradation of 4-NP, *Catalysts*, 2020, **10**, 1437.

122 M. N. Khan, O. Bashir, T. A. Khan, S. A. Al-Thabaiti and Z. Khan, Catalytic Activity of Cobalt Nanoparticles for Dye and 4-Nitro Phenol Degradation: A Kinetic and Mechanistic Study, *Int. J. Chem. Kinet.*, 2017, **49**, 438–454.

123 B. Abebe, H. C. A. Murthy and E. Amare, Summary on Adsorption and Photocatalysis for Pollutant Remediation: Mini Review, *J. Encapsulation Adsorpt. Sci.*, 2018, **08**, 225–255.

124 Z. Zhang and Y. Wu, Investigation of the NaBH4-Induced aggregation of Au nanoparticles, *Langmuir*, 2010, **26**, 9214–9223.

125 R. L. Wang, D. P. Li, L. J. Wang, X. Zhang, Z. Y. Zhou, J. L. Mu and Z. M. Su, The preparation of new covalent organic framework embedded with silver nanoparticles and its applications in degradation of organic pollutants from waste water, *Dalton Trans.*, 2019, **48**, 1051–1059.

126 H. Li, G. T. Fei, M. Fang, P. Cui, X. Guo, P. Yan and L. De Zhang, Synthesis of urchin-like Co 3 O 4 hierarchical micro/nanostructures and their photocatalytic activity, *Appl. Surf. Sci.*, 2011, **257**, 6527–6530.

127 Y. Zhang, P. Zhu, L. Chen, G. Li, F. Zhou, D. Lu, R. Sun and C. P. Wong, Hierarchical architectures of monodisperse porous Cu microspheres: Synthesis, growth mechanism, high-efficiency and recyclable catalytic performance, *J. Mater. Chem. A*, 2014, **2**, 11966–11973.

128 X.-Z. Li, K.-L. Wu, Y. Ye and X.-W. Wei, Controllable synthesis of Ni nanotube arrays and their structure-dependent catalytic activity toward dye degradation, *CrystEngComm*, 2014, **16**, 4406–4413.

129 A. Corma and H. Garcia, Silica-Bound Homogenous Catalysts as Recoverable and Reusable Catalysts in Organic Synthesis, *Adv. Synth. Catal.*, 2006, **348**, 1391–1412.

130 X. Yang, H. Zhong, Y. Zhu, H. Jiang, J. Shen, J. Huang and C. Li, Highly efficient reusable catalyst based on silicon nanowire arrays decorated with copper nanoparticles, *J. Mater. Chem. A*, 2014, **2**, 9040–9047.

131 A. Ajmal, I. Majeed, R. N. Malik, H. Idriss and M. A. Nadeem, Principles and mechanisms of photocatalytic dye degradation on TiO2 based photocatalysts: a comparative overview, *RSC Adv.*, 2014, **4**, 37003–37026.

132 A. F. Alkaim, A. M. Aljeboree, N. A. Alrazaq, S. J. Baqir, F. H. Hussein and A. J. Lilo, Effect of pH on adsorption and photocatalytic degradation efficiency of different catalysts on removal of methylene blue, *Asian J. Chem.*, 2014, **26**, 8445–8448.

133 M. M. Haque and M. Muneer, Photodegradation of norfloxacin in aqueous suspensions of titanium dioxide, *J. Hazard. Mater.*, 2007, **145**, 51–57.

134 H. Wang, C. Xie, W. Zhang, S. Cai, Z. Yang and Y. Gui, Comparison of dye degradation efficiency using ZnO powders with various size scales, *J. Hazard. Mater.*, 2007, **141**, 645–652.

135 H. Zhu, R. Jiang, Y. Fu, Y. Guan, J. Yao, L. Xiao and G. Zeng, Effective photocatalytic decolorization of methyl orange utilizing TiO 2/ZnO/chitosan nanocomposite films under simulated solar irradiation, *Desalination*, 2012, **286**, 41–48.

136 A. H. Mahvi, M. Ghanbarian, S. Nasseri and A. Khairi, Mineralization and discoloration of textile wastewater by TiO2 nanoparticles, *Desalination*, 2009, **239**, 309–316.

137 S. K. Kansal, M. Singh and D. Sud, Studies on TiO2/ZnO photocatalysed degradation of lignin, *J. Hazard. Mater.*, 2008, **153**, 412–417.

138 E. C. Ilinoiu, R. Pode, F. Manea, L. A. Colar, A. Jakab, C. Orha, C. Ratiu, C. Lazau and P. Sfarloaga, Photocatalytic activity of a nitrogen-doped TiO2 modified zeolite in the degradation of Reactive Yellow 125 azo dye, *J. Taiwan Inst. Chem. Eng.*, 2013, **44**, 270–278.

139 S. Ullah, Q. Li, R. Ullah, S. Anwar, M. F. Hameed and M. Zhu, Facile synthesis of water-soluble silver nanoclusters for the photocatalytic degradation of dyes by multivariate optimization approach, *Nanoscale Adv.*, 2023, **5**, 3326–3335.

140 T. Goswami, M. Singh, K. M. Reddy and A. K. Mishra, Facile Synthesis of Ag-TiO2 Hybrid Nanocluster:A Comprehensive Experimental and Computational Insight into the Role of Surface Ligands on Enhanced Visible Light Photocatalysis, *ChemistrySelect*, 2018, **3**, 10892–10899.

141 T. Goswami, A. Bheemaraju, A. K. Sharma and S. Bhandari, Perylenetetracarboxylic acid–incorporated silver nanocluster for cost-effective visible-light-driven photocatalysis and catalytic reduction, *Colloid Polym. Sci.*, 2021, **299**, 925–936.

142 M. Ghali, M. Benltifa, C. Brahmi, L. Elbassi, F. Dumur, C. Simonnet-Jégat, L. Bousselmi and J. Lalevée, LED and solar photodecomposition of erythrosine B and rose Bengal using H3PMo12O40/polymer photocatalyst, *Eur. Polym. J.*, 2021, **159**, 110743.

143 L. Chen, F. He, N. Zhao and R. Guo, Fabrication of 3D quasi-hierarchical Z-scheme RGO-Fe 2 O 3 -MoS 2 nanoheterostructures for highly enhanced visible-light-driven photocatalytic degradation, *Appl. Surf. Sci.*, 2017, **420**, 669–680.

144 S. Kalele, A. C. Deshpande, S. B. Singh and S. K. Kulkarni, Tuning luminescence intensity of RHO6G dye using silver nanoparticles, *Bull. Mater. Sci.*, 2008, **31**, 541–544.

145 N. Gupta, H. P. Singh and R. K. Sharma, Metal nanoparticles with high catalytic activity in degradation of methyl orange: An electron relay effect, *J. Mol. Catal. A:Chem.*, 2011, **335**, 248–252.

146 K. Wannakan, K. Khansamrit, T. Senasu, T. Chankhanittha and S. Nanan, Ag-Modified ZnO for Degradation of

Oxytetracycline Antibiotic and Reactive Red Azo Dye, *Antibiotics*, 2022, **11**(11), 1590.

147 Z. Yu, F. Li and L. Sun, Recent advances in dye-sensitized photoelectrochemical cells for solar hydrogen production based on molecular components, *Energy Environ. Sci.*, 2015, **8**, 760–775.

148 H. Li, Xi Kang and M. Zhu, Nanocluster-based aggregates: Assembled forms, driving forces, and structure-related properties, *Coord. Chem. Rev.*, 2025, **539**, 216738.

149 N. Mzimela, S. Tichapondwa and E. Chirwa, Visible-light-activated photocatalytic degradation of rhodamine B using WO3 nanoparticles, *RSC Adv.*, 2022, **12**, 34652–34659.

150 H. Tedla, M. Goddati, E. B. Wondemagegnehu, L. T. Tufa, A. Mekonnen and J. Lee, Phytoextract-assisted synthesis of Fe2O3/MgO nanocomposites for efficient photocatalytic degradation of gentian violet, *Front. Environ. Chem.*, 2024, **5**, 1323752.

151 K. Michalec, B. Mozgawa, A. Kusior, P. Pietrzyk, Z. Sojka and M. Radecka, Tunable Generation of Reactive Oxygen Species in SnO2/SnS2 Nanostructures: Mechanistic Insights into Indigo Carmine Photodegradation, *J. Phys. Chem. C*, 2024, **128**, 5011–5029.

152 Z. Zhang and Y. Wu, Investigation of the NaBH4-Induced aggregation of Au nanoparticles, *Langmuir*, 2010, **26**, 9214–9223.

153 M. Sahin and I. H. Gubbuk, Green synthesis of palladium nanoparticles and investigation of their catalytic activity for methylene blue, methyl orange and rhodamine B degradation by sodium borohydride, *React. Kinet., Mech. Catal.*, 2022, **135**, 999–1010.

154 N. T. K. Thanh, N. Maclean and S. Mahiddine, Mechanisms of nucleation and growth of nanoparticles in solution, *Chem. Rev.*, 2014, **114**, 7610–7630.

155 K. Zhang, J. M. Suh, J. W. Choi, H. W. Jang, M. Shokouhimehr and R. S. Varma, Recent Advances in the Nanocatalyst-Assisted NaBH4 Reduction of Nitroaromatics in Water, *ACS Omega*, 2019, **4**, 483–495.